E.O. Paton Electric Welding Institute of the National Academy of Sciences of Ukraine

International Scientific-Technical and Production Journal

The Paton WELDING JOURNAL

Issue 7 2021

Published Monthly Since 2000

English Translation of the Monthly «Avtomatychne Zvaryuvannya» (Avtomaticheskaya Svarka/Automatic Welding) Journal Published in Ukrainian and Russian Since 1948

Founders
E.O. Paton Electric Welding Institute
International Association «Welding»

Publisher
International Association «Welding»

Translators
A.O. Fomin, I.M. Kutianova
Editor
N.G. Khomenko
Electron galley
D.I. Sereda, T.Yu. Snegiryova

Address
E.O. Paton Electric Welding Institute,
International Association «Welding»
11 Kazymyr Malevych Str. (former Bozhenko),
03150, Kyiv, Ukraine
Tel.:/Fax: (38044) 200 82 77
E-mail: journal@paton.kiev.ua
www://patonpublishinghouse.com/eng/journals/tpwj

State Registration Certificate
KV 4790 of 09.01.2001
ISSN 0957-798X
DOI: http://dx.doi.org/10.37434/tpwj

Subscriptions
12 issues per year, back issues available.
$384, subscriptions for the printed (hard copy) version, air postage and packaging included.
$312, subscriptions for the electronic version (sending issues of Journal in pdf format or providing access to IP addresses).
Institutions with current subscriptions on printed version can purchase online access to the electronic versions of any back issues that they have not subscribed to.
Issues of the Journal (more than two years old) are available at a substantially reduced price.

CONTENTS

https://doi.org/10.37434/tpwj2021.07.01

PROPERTIES OF BUTT JOINTS OF FINE-SHEET ALUMINIUM-LITHIUM 1460 ALLOY, PRODUCED BY FRICTION STIR AND TIG WELDING

A.G. Poklyatskyi, S.I. Motrunich and **O.S. Kushnaryova**
E.O. Paton Electric Welding Institute of the NAS of Ukraine
11 Kazymyr Malevych Str., 03150, Kyiv, Ukraine. E-mail: office@paton.kiev.ua

The article analyzes the structural features, characteristics of strength and life of butt joints of aluminium-lithium 1460 alloy with a thickness of 2 mm, produced by friction stir welding and argon arc welding using nonconsumable electrode. It is shown that friction stir welding prevents the formation of a coarse-dendritic structure of welds, provides the formation of permanent joints with a minimum level of stress concentration at the place of transition from the weld to the base material and allows avoiding defects in the welds in the form of pores, oxide film and hot cracks, caused by melting and crystallization of metal during fusion welding. 16 Ref., 7 Figures.

K e y w o r d s : aluminium-lithium 1460 alloy, friction stir welding, hardness, defects, microstructure, tensile strength, fatigue resistance, fine structure

Light, durable and corrosion-resistant aluminium-lithium alloys have a low density and a high modulus of elasticity, which allows them to be widely applied in the creation of aircraft and rocket space engineering. 1460 alloy of the alloying system Al–Cu–Li (nominal composition is 3 % Cu; 2 % Li) with the addition of zirconium and scandium is the most high-strength (> 500 MPa at a density of 2.6 g/cm^3). A simultaneous increase in the values of strength and ductility of this alloy at ultra-low temperatures makes it promising for manufacture of welded cryogenic tanks [1–3]. In most cases, to produce permanent joints different methods of fusion welding are used. A weld is formed as a result of melting a certain volume of joined materials and filler wire in the common welding pool and their crystallization. This leads to significant structural transformations both in the weld metal as well as in the adjacent areas of the base material, as well as the formation of typical defects in the form of pores, macroinclusions of oxide films and hot crystallization cracks. Therefore, the tensile strength of such welded joints in most cases does not exceed 70% of this value for the base material [4, 5].

During friction stir welding (FSW), the weld is formed in the solid phase due to heating of a small volume of metal to a ductile state as a result of friction and stirring it across the entire thickness of the welded edges with the working surfaces of a special tool. Due to that it is possible to avoid the problems caused by melting and crystallization of metal, and to keep the properties of semi-finished products in welded assemblies applied at their manufacturing as much as possible [6, 7]. As compared to fusion welding, among the main advantages of FSW process there are formation of fine-crystalline structure of joints and complete preservation of alloying elements in them, absence of pores, oxide inclusions and hot cracks, reduction of metal softening in the welding zone and the level of residual stresses and strains in the joints, as well as increase in their tensile strength under static tension and fatigue resistance under cyclic loads [8–11].

The aim of the work is to evaluate the advantages of FSW process over argon arc welding using nonconsumable electrode (AAWNE) in producing butt joints of thin-sheet aluminium-lithium 1460 alloy.

For investigations, sheets of aluminium-lithium 1460 alloy with a thickness of 2 mm were used. Butt joints were produced by argon arc welding using nonconsumable electrode at a speed of 20 m/h at a current of 145 A in the MW-450 welding installation («Fronius», Austria) with the use of the filler wire Sv1201 of 1.6 mm diameter. FSW was performed in a laboratory installation designed by the E.O. Paton Electric Welding Institute, using a special tool with a conical tip and a bead of 12 mm diameter [12], the speed of rotation of which was 1420 rpm, and the speed of linear movement was 14 m/h. The produced welded joints were used to make microsections for the study of structural features of welds and specimens with a width of working part being 15 mm to determine their tensile strength at a uniaxial tension in accordance with DSTU EN ISO 4136x. The specimens produced by AAWNE were tested both with the melts removed

A.G. Poklyatskyi — https://orcid.org/0000-0002-4101-2206, S.I. Motrunich — https://orcid.org/orcid.org/0000-0002-8841-8609, O.S. Kushnaryova — https://orcid.org/0000-0002-2125-1795

to the level of the base material and with additionally cleaned weld reinforcements. The width of the working part of the specimens to determine fatigue resistance was 25 mm. Mechanical tests of the specimens were performed in the universal servohydraulic complex MTS 318.25. Cyclic tests were performed at an axial regular loading at a load cycle asymmetry coefficient $R_\sigma = 0.1$ and a frequency of 15 Hz until a complete fracture of the specimens. Under the same conditions, 5–7 specimens of the same type were tested. The experimental data of fatigue tests were processed by the methods of linear regression analysis, typical for this type of tests. Based on the obtained results, a corresponding fatigue curve was constructed for each series of specimens on the basis of the established limits of fatigue resistance — regression line of experimental data in the coordinates $2\sigma_a$ – lg/N. The hardness of metal was measured on the facial surface of the cleaned joints. The degree of softening the metal in the welding zone was evaluated in the device ROCKWELL at a load of $P = 600$ N. Evaluation of structural features of welded joints was carried out by means of the optical (MIM-8) and transmission microdiffraction electron microscopy (JEM-200CX). Thin foils for «transmission» were prepared by a two-stage method — preliminary electropolishing and a subsequent multiple ion thinning by ionized argon fluxes in a special installation [13], which allowed making all structural-phase components of the studied welds «transparent» for electrons.

As a result of the carried out investigations it was established that due to the formation of permanent joints on a substrate without a groove and without the use of a filler wire, the welds produced in FSW as to the shape and sizes favourably differ from the welds produced by fusion (Figure 1). The absence of penetrations and reinforcements on such welds allows avoiding high levels of stress concentration in the places of transition from a weld to the base material, which negatively influence the operational and life characteristics of welded joints.

In addition, the formation of permanent joints in the solid phase without melting the base material prevents the appearance of defects in the form of pores typical for fusion welding (see Figure 1, *b*, *d*). The absence of molten metal in the welding zone, in which the solubility of hydrogen increases sharply, avoids the additional saturation by it of this zone as a result of migration of this gas from the adjacent metal layers, whereas stirring and thickening of the welded metal in the zone of permanent joint formation provides producing welds without pores.

Deformation and intensive stirring of the plasticized metal throughout the entire thickness of the welded edges promotes the refinement of oxide films, which are instantly formed on them even after mechanical removal immediately before welding,

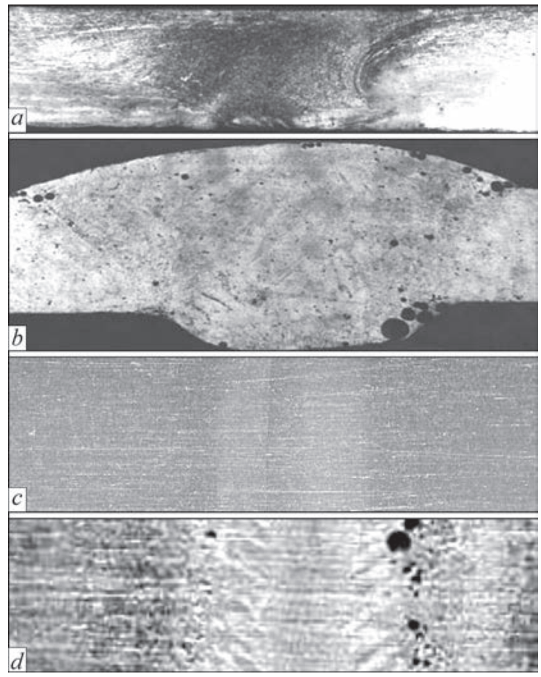

Figure 1. Cross-sections (*a*, *b*) and root parts (*c*, *d*) of welds of 1460 alloy of 2 mm thickness, produced by FSW (*a*, *c*) and AAWNE (*b*, *d*)

whereas the absence of molten metal in the area of the permanent joint formation avoids its oxidation during welding. Therefore, in the welds produced by FSW, defects in the form of separate or extended [14, 15] macroinclusions of oxide films typical for the welds produced by AAWNE of aluminium-lithium 1460 alloy are absent (Figure 2).

The most dangerous and inadmissible defects for structures of critical purpose are hot cracks, which are quite often formed in the process of crystallization of molten metal at the place of accumulation of low-melting eutectic inclusions. During fusion welding of aluminium alloys, such crystallization cracks can occur both in the weld metal as well as in the area of its fusion with the base material. The carried out investigations showed that in AAWNE of special Holdcroft specimens, which allow evaluating hot brittleness of alu-

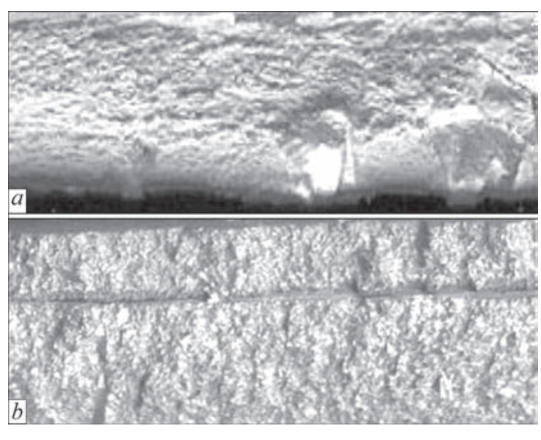

Figure 2. Defects in the form of typical separate (*a*) and elongated (*b*) macroinclusions of oxide films on longitudinal fractures of welds of 1460 alloy of 2 mm thickness, produced by AAWNE

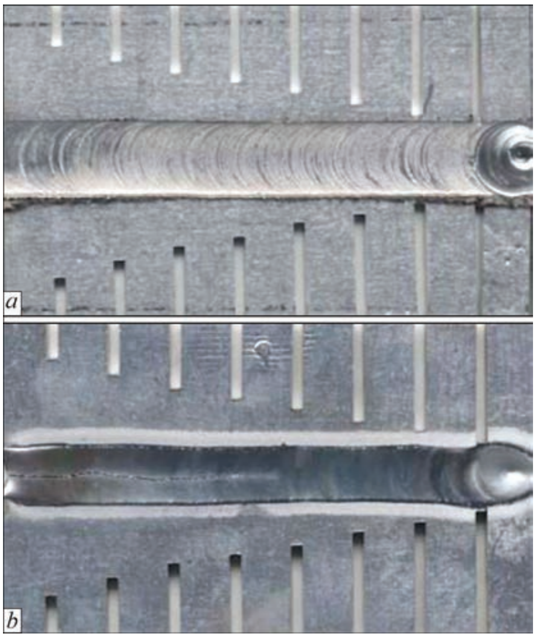

Figure 3. Holdcroft specimens of 1460 alloy of 2 mm thickness, welded by FSW (*a*) and AAWNE (*b*)

minium alloys during fusion welding without the use of filler wire, hot cracks are formed in the central part of the welds (Figure 3). Of course, in case of FSW of such specimens hot cracks cannot appear, as far as welding occurs in the solid phase, when the processes of metal fusion and crystallization are completely absent.

Analysis of the microstructure of welded joints of aluminium-lithium 1460 alloy, produced by AAWNE, showed that the weld metal has a mainly fine-crystalline structure with manifestations of central crystallite in some parts of individual fragments (Figure 4). Near the zone of fusion of the weld with the base material, a layer with a small subdendritic structure is observed in it (Figure 4, *b*–*d*). In the heat-affected zone (HAZ) near the zone of fusion of the weld with the base material there are areas of overheating and recrystallization. The length of the melting zone of the structural components is about 2.25 mm from the fusion boundary of the weld with the base material. In the HAZ, the grains that are directly adjacent to the abovementioned zone have the largest size.

When this alloy is welded by friction stir method, in the central part (core) of the weld, as a result of intensive plastic deformation of the metal, very fine (3–5 μm), equiaxed grains are formed (Figure 4 *d*, *e*, *f*). In the zone of thermomechanical impact, a smooth change of grain orientation in the direction of movement of working surfaces of the tool occurs. As a result, long elongated grains are formed in it, oriented along this trajectory, as well as small equiaxed grains.

Analysis of the fine structure of the weld metal produced by AAWNE and FSW showed that in both cases two types of phase precipitations are formed. Some of them (grain boundary phases or phases of intergranular type), which are located along the intergranular boundaries, are represented by eutectic formations (Figure 5). Another type of phase formations is intergranular phase precipitations or phases of intergranular type. The welding method significantly affects the size of such phase precipitations. Thus, in the welds produced by fusion, grain boundary phases can have a thickness of up to 0.2–0.5 μm and a rather considerable elongation (up to 2.0–2.5 μm). Phases of the intergranular type differ in a globular shape and can be 6 times higher than similar precipitations in the base material. In the welds produced by friction stir welding, the sizes of phase precipitations are by 2.5–3.5 times smaller. At the same time, a significant increase in their amount at a uniform distribution both over intergranular as well as over grain boundary volumes is observed. In addition, a significant part of phase precipitations is surrounded by a near-phase shell,

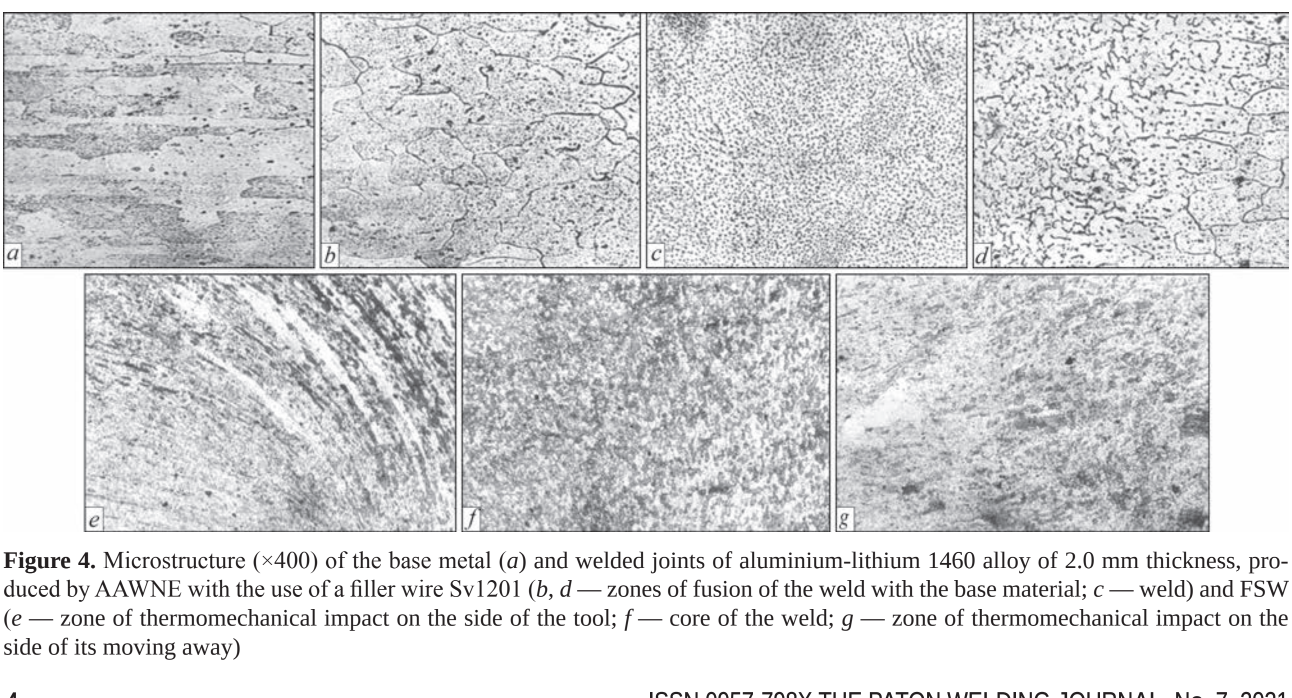

Figure 4. Microstructure (×400) of the base metal (*a*) and welded joints of aluminium-lithium 1460 alloy of 2.0 mm thickness, produced by AAWNE with the use of a filler wire Sv1201 (*b*, *d* — zones of fusion of the weld with the base material; *c* — weld) and FSW (*e* — zone of thermomechanical impact on the side of the tool; *f* — core of the weld; *g* — zone of thermomechanical impact on the side of its moving away)

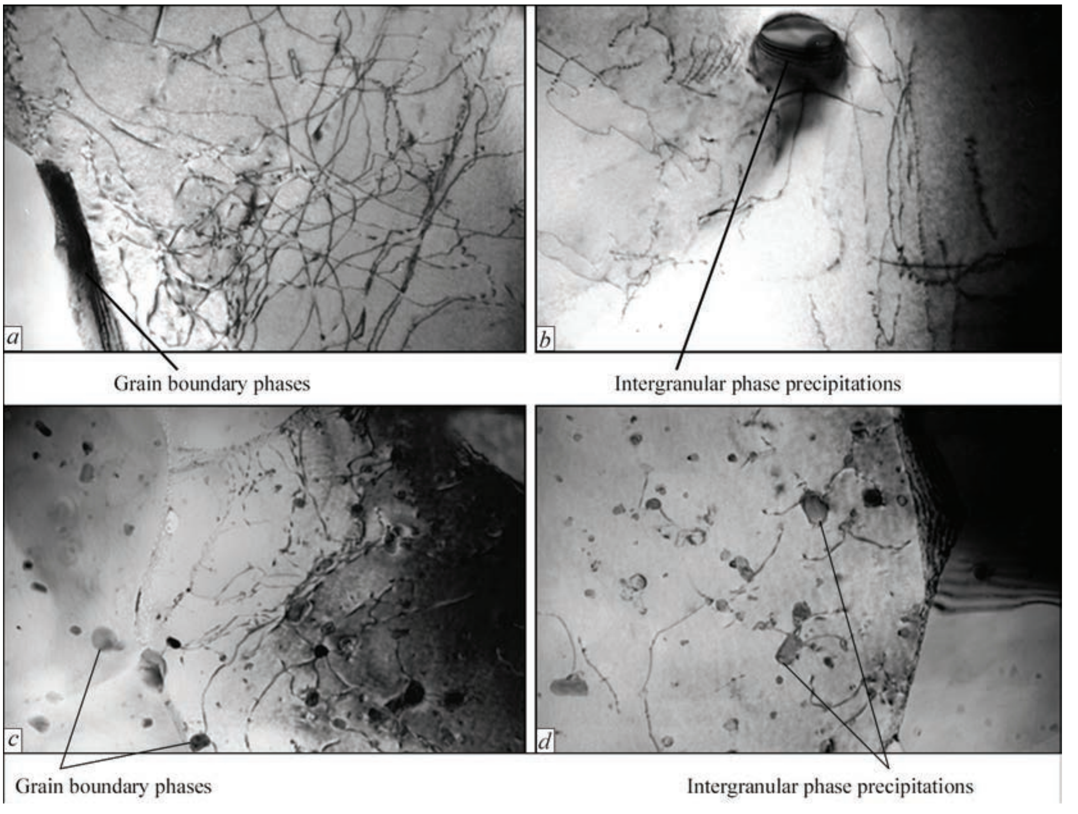

Figure 5. Fine structure of weld metal of aluminium-lithium 1460 alloy produced by AAWNE (*a*, *b*) and FSW (*c*, *d*) with the grain boundary phases (*a*, *c*) and intergranular phase precipitations (*b*, *d*), typical for these methods of producing permanent joints (*b*, *d*): *a*, *b*, *d* — 30000; *c* — 20000

which may indicate an intensive alloying of a local near-phase space in the volumes of matrix grains.

Due to a lower temperature of heating welded edges and the formation of fine-crystalline weld structure, in the process of FSW, the level of softening of the metal is less than in AAWNE (Figure 6). Therefore, as a result of measurements of hardness of metal in different areas of welded joints it was established that the minimum hardness of weld metal produced by AAWNE with the use of a filler wire Sv1201 amounts to *HRB* 71, and in the zones of its fusion with the base material it is *HRB* 82–83. Whereas, in FSW the hardness of the metal in the weld and its zones of mating with the base material is at the level of *HRB* 85–86.

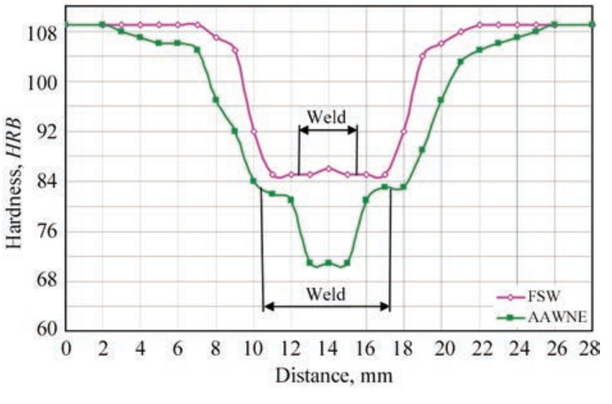

Figure 6. Distribution of hardness in welded joints of 1460 alloy of 2 mm thickness, produced by FSW and AAWNE

Therefore, in the case of uniaxial static tension, the specimens of welded joints without reinforcement of the weld, produced by AAWNE with the use of a filler wire Sv1201, are fractured along the weld metal and have the lowest (257 MPa) strength. The fracture of welded joint specimens produced by FSW occurs in the zone of thermomechanical impact. In this case, their tensile strength is at the level of 310 MPa as in the specimens with the weld reinforcement produced by AAWNE, which are fractured in the area of fusion of the weld with the base material.

The experimentally determined fatigue curves of butt joints of aluminium-lithium 1460 alloy produced

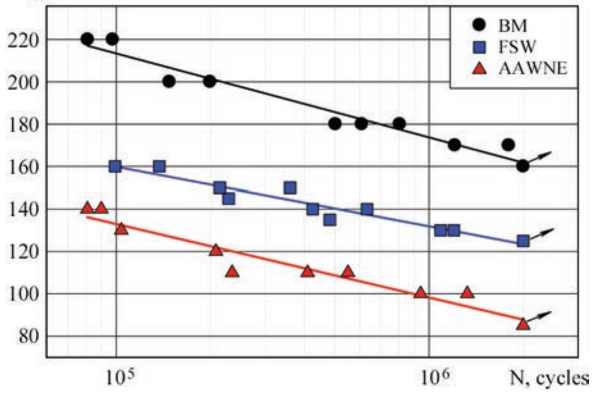

Figure 7. Fatigue curves of base metal and welded joints of aluminium-lithium 1460 alloy of 2 mm thickness at an asymmetry of the stress cycle $R_\sigma = 0.1$

by FSW indicate a high fatigue resistance of such joints [16]. The limits of fatigue strength of specimens of the joints of aluminium 1460T1 alloy produced by FSW at an asymmetry of a cycle of stresses $R_\sigma = 0.1$ amount to 75–77 % of the corresponding indices of the base metal in the entire area of life of 10^5–$2{\cdot}10^6$ of stress change cycles and for the base 10^5 and $2{\cdot}10^6$ amount to 160 and 123 MPa, respectively (Figure 7). The limit of fatigue resistance on the base $2{\cdot}10^6$ of stress change cycles for the joints produced by AAWNE do not exceed 88 MPa, which is by 28 % lower than the same index for the joints produced by FSW.

Conclusions

1. The FSW process provides the formation of permanent joints of aluminium-lithium 1460 alloy with a minimum level of stress concentration at the places of transition from the weld to the base material and allows preventing the formation of defects in the welds in the form of pores, macroinclusions of oxide films and hot cracks typical for AAWNE and those predetermined by melting and crystallization of metal.

2. The formation of permanent joints in the solid phase allows avoiding the formation of a cast coarse-dendritic structure of the welds, inherent in the processes of fusion welding. At the same time, around the tip of the tool, where the metal experiences the greatest thermomechanical impact, due to its intense plastic deformation a refinement of grains and the formation of a new homogeneous disoriented structure in the weld core with a grain size of 3–5 μm and dispersed (0.06–0.40 μm) eutectic phase precipitations occur. Near the core in the zone of thermomechanical impact a combined zone is formed, which contains small equiaxed grains and deformed thin elongated grains, oriented along the direction of movement of the working surfaces of the tool.

3. In FSW of thermally strengthened aluminium-lithium 1460 alloy as a result of thermomechanical impact besides a refinement of grains in a welding zone, which promotes an increase in the hardness of metal, at the same time a partial precipitation of excessive phases from a supersaturated solid solution and their coagulation occurs, as a result of which a hardness of metal is slightly reduced. However, the degree of softening the metal in the zone of a permanent joint formation in FSW is much lower than in AAWNE. Due to that, the tensile strength of the specimens of welded joints produced by FSW is at the same level with this index for the specimens with the weld reinforcement and is by 20 % higher than for the specimens without the weld reinforcement, produced by AAWNE with the use of a filler wire Sv1201.

4. As a result of experimental studies, it was found that the butt joints of aluminium-lithium 1460 alloy, produced by FSW, have a high fatigue resistance and can be successfully used in structures operated under variable loads. The limits of fatigue resistance of the specimens of welded joints at an asymmetry of a cycle of stresses $R_\sigma = 0.1$ amount to 75–77 % from the corresponding indices of base metal in the entire area of life of 10^5–$2{\cdot}10^6$ of stress change cycles and for the base $2{\cdot}10^6$ it amount to 123 MPa.

1. Bratukhin, A.G. (2003) *Modern aircraft materials: Technological and functional peculiarities.* Moscow, Aviatekhinform [in Russian].
2. Beletsky, V.M., Krivov, G.A. (2005) *Aluminium alloys (composition, properties, technology, application):* Refer. Book. Ed. by I.N. Fridlyander. Kiev, KOMINTEKh [in Russian].
3. (2002) *Aircraft materials. Selected works of VIAM for 1932–2002:* Jubilee Sci.-Techn. Collect. Ed. by E.N. Kablov. Moscow, MISIS VIAM, 198–220 [in Russian].
4. Rabkin, D.M., Lozovskaya, A.V., Sklabinskaya, I.E. (1992) *Physical metallurgy of welding of aluminium and its alloys.* Ed. by V.N. Zamkov. Kiev, Naukova Dumka [in Russian].
5. Mashin, V.S., Poklyatsky, A.G., Fedorchuk, V.E. (2005) Mechanical properties of aluminium alloys in consumable and nonconsumable electrode arc welding. *The Paton Welding J.*, **9**, 39–45.
6. Thomas, W.M., Nicholas, E.D., Needham, J.C. et al. (1991) *Friction stir butt welding.* Int. Pat. Appl. PCT/GB 92/02203; GB Pat. Appl. 9125978.8.
7. Dawes, C.J., Thomas, W.M. (1996) Friction stir process welds aluminum alloys. *Welding J.*, **3**, 41–45.
8. Defalco, J. (2006) Friction stir welding vs. fusion welding. *Ibid*., **3**, 42–44.
9. Ericsson, M., Sandstrom, R. (2003) Influence of melting speed on the fatigue of friction stir welds, and comparison with MIG and TIG. *Int. J. Fatigue*, **25**, 1379–1387.
10. Enomoto, M. (2003) Friction stir welding: Research and industrial applications. *Welding Intern.*, **5**, 341–345.
11. Larsson, H., Karlsson, L., Svensson, L. (2000) Friction stir welding of AA5083 and AA6082 aluminium alloys. *Svetsaren*, **2**, 6–10.
12. Ishchenko, A.Ya., Poklyatsky, A.G. (2010) *Tool for friction stir welding of aluminium alloys* Pat. 54096, Int. Cl. B23K 20/12; u201005315; Filled 30.04.2010; Publ. 25.10, PWI [in Ukrainian].
13. Darovsky, Yu.F., Markashova, L.I., Abramov, N.P. et al. (1985) Procedure of thinning of permanent welded joint samples for electron microscopic examinations. *Avtomatich. Svarka*, **12**, 60 [in Russian].
14. Poklyatsky, A.G., Lozovskaya, A.V., Grinyuk, A.A. (2002) Prevention of formation of oxide films in welds on Li-containing aluminium alloys. *The Paton Welding J.*, **12**, 39–42.
15. Lukianenko, A., Motrunich, S., Labur, T. et al. (2020) Mechanical properties of welded thin sheets of Al–Cu–Li alloy and noise level assessment during FSW and TIG welding. *FME TRANSACTIONS*, 49(**1**), 220–224.
16. Motrunich, S., Klochkov, I., Poklyatsky, A. (2020) High cycle fatigue behaviour of thin sheet joints of aluminium–lithium alloys under constant and variable amplitude loading. *Weld World*, **64**, 1971–1979.

Received 20.05.2021

https://doi.org/10.37434/tpwj2021.07.02

INFLUENCE OF OXYGEN CONCENTRATION IN ARGON OF THE PROTECTIVE NOZZLE ON THE PROPERTIES AND COLOUR OF WELD SURFACE IN TIG WELDING OF TITANIUM

V.P. Prilutskyi and **I.K. Petrichenko**
E.O. Paton Electric Welding Institute of the NAS of Ukraine
11 Kazymyr Malevych Str., 03150, Kyiv, Ukraine. E-mail: office@paton.kiev.ua

The paper presents the results of investigations of the process of formation of a gas-saturated layer on the weld surface at accidental violation of the conditions of argon protection (under the nozzle) in TIG welding of VT1-0 titanium. It was found that the change of oxygen content in argon of the protective nozzle in the range from 0.024 to 1.18 vol.% leads to a change of the colour of a region of forming weld surface. It is shown that each colour corresponds to a certain depth of the gas-saturated layer that can be up to 0.25 mm. A correlation dependence of weld surface colour–gas-saturated layer thickness–oxygen content in the protective nozzle was established. Results of gas analysis and mechanical testing of the welds show that oxygen and nitrogen from the air in the argon of the protective nozzle practically do not interact with the molten metal of the weld pool during welding. Therefore, the quantitative characteristics of the metal of welds are on the level of those of the welds produced under standard conditions. To increase the operational reliability of welded assemblies with a coloured surface of a weld region, it is proposed to remove it, depending on its colour, to the depth in the range from 0.10 up to 0.25 mm. 9 Ref., 2 Tables, 6 Figures.

Keywords: argon-arc welding (TIG), VT1-0 titanium alloy, weld surface colour, violation of argon protection, weld metal properties

Tungsten electrode inert-gas (TIG) welding became widely accepted in industry for fabrication of titanium structures. The activity of titanium interaction with atmospheric gases, namely oxygen, nitrogen, carbon dioxide gas, moisture vapours, which are harmful impurities for titanium, becomes higher with increase of temperature. Noticeable absorption of oxygen by titanium begins already at the temperature of 300 °C, that of nitrogen — at 800 °C [1]. Oxygen solubility in α-phase can reach 34 at.%, that of nitrogen — 0.75 at.%, here the speed of titanium interaction with oxygen is 50 times higher than that of interaction with nitrogen [2]. High-temperature interaction of titanium with the air environment is accompanied by oxygen diffusion in-depth of the matrix and formation of solid solution of oxygen and nitrogen in titanium, which leads to pronounced distortion of the crystalline lattice and, as a result, to deterioration of mechanical characteristics of metal. The oxide layer which formed on the surface as a coarse acicular α′-phase, has higher hardness and brittleness [3]. Note that interstitial impurities not only have the strongest influence on titanium alloy weldability, but also promote delayed fracture of welded structures, in connection with formation of cold cracks in the welds and heat-effect zone (HAZ) [4, 5]. Therefore, in TIG welding special attention is given to reliable protection from contact with air not only of the weld pool molten metal, but also of the cooling welded joint [6]. To eliminate weld metal contamination by harmful impurities, in addition to application of high-purity argon, also welding torches and protective devices are used, which provide high-quality protection of the entire welded joint zone by inert gas. Correct selection of the ratio of argon flow rate to the welding torch and protective nozzle is important here. However, despite the high-quality protection, accidental violations of argon protection may occur during welding, both in the arc burning zone under the torch orifice, and in the zone of the cooling welded joint. Work [7] describes a method that allows revealing the violations of argon protection in the arc burning zone during welding and determining the degree of the influence of this violation on the weld mechanical properties. However, it is practically impossible to establish a violation of argon protection of the cooling weld surface, using such a procedure. Such a violation can be revealed only when the weld moves out from under the protective nozzle. When all the technological requirements to the welding process are followed, the weld surface has a silvery colour, while the change of the conditions of argon protection under the nozzle leads to a change of the weld surface colour, as a result of formation

V.P. Prilutskyi — https://orcid.org/0000-0002-3174-1966

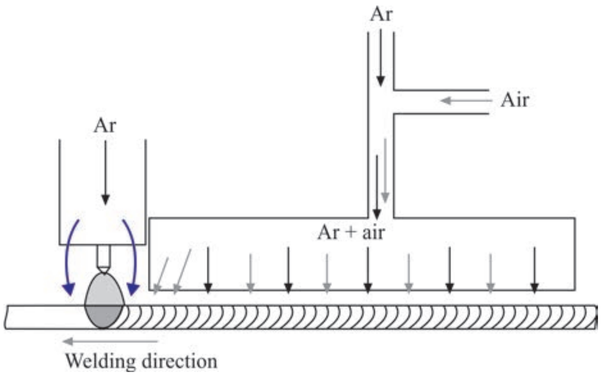

Figure 1. Scheme of air feeding into the protective nozzle

of an oxide-nitride layer of titanium on it. Such an effect is currently considered as a characteristic of the properties and performance of the welded joint. Thus, a standard was proposed, according to which the weld surface colour is the only characteristic for assessment of fitness for service of structures with such welds [8]. There is no information in publications on substantiation of quantitative assessment of the properties of the region of weld metal with a coloured surface. Therefore, investigation of the influence of random increase of oxygen content in the protective nozzle argon on the properties of weld metal at the change of its surface colour is an urgent problem. Its solution will allow creation of a data base: weld surface colour–weld metal properties, the objective of which is increasing the operational reliability of welded structure components, where coloured regions were revealed on the weld surface.

Procedure and materials. A package of methods was used for quantitative assessment of the influence of the concentration of interstitial impurities (oxygen and nitrogen) in the protective nozzle argon on weld metal properties, depending on the colour of their surface:

- spectral analysis;
- photographing the colour of weld surface;
- metallographic analysis;
- measurement of weld metal microhardness;
- determination of gas content in weld metal;
- mechanical tests of weld metal.

Table 1. Content of air (oxygen and nitrogen) in the protective nozzle argon, vol.%

Sample index	Air content	Oxygen content	Nitrogen content
1	0.12	0.024	0.09
2	0.19	0.038	0.14
3	0.37	0.074	0.28
4	0.48	0.096	0.37
5	0.60	0.120	0.46
6	1.10	0.220	0.85
7	1.60	0.320	1.24
8	2.24	0.440	1.74
9	5.90	1.180	4.60

Spectral analysis. Oxygen presence in the arc gap was determined by the intensity of radiation of oxygen atomic lines by the procedure, described in work [7]. A dosed amount of air was added to argon, coming to the protective nozzle. Air was fed to argon by the scheme shown in Figure 1.

An optimum ratio between argon flow rate to the torch and nozzle that ensures the required quality, was determined experimentally, trying to obtain the silver colour of the weld. Welding modes were as follows: welding current of 160 A, welding speed of 12 m/h, arc gap length of 1.5 mm. Argon flow rate to the torch was 12 l/min, to protective nozzle — 27 l/min. Air content in argon of the protective nozzle was varied in the range of 0.12–5.9 vol.%, here oxygen content changed in the range of 0.024–1.18 vol.% (Table 1). Welding was performed on 3 mm sheets of titanium alloy of VT1-0 grade. To ensure high-quality protection of the cooling HAZ metal, the distance from the protective nozzle plane to sheet surface was within 1.0–1.5 mm. Not less than three samples were welded at each value of air concentration, and the average value of radiation intensity of oxygen atomic lines was determined.

Photographing of weld surface was performed with digital camera of CANON model. Filming conditions (exposure, lighting, distance to weld surface) were the same for all the welded samples. After welding with each variant of oxygen concentration in argon of the protective nozzle, the weld surface was photographed to obtain the following correlation dependence: weld surface colour–weld metal properties.

Metallographic analysis. Increase of air content in argon of the protective nozzle leads to formation of oxide-nitride superfine films of different colour on the weld surface. The thickness of such films can be assessed by interference coloration [9]. Located under the colour film is metal with higher oxygen and nitrogen content, where the crystalline lattice is distorted and coarse acicular α′-phase is formed. Investigation of changes in microstructure in the surface layer of the metal of welds, made at fixed values of oxygen concentration in argon of the protective nozzle was performed in NEOPHOT-2 microscope.

Microhardness of the surface layer of weld metal was measured layer-by-layer by PMT-3 instrument at 50 g load. On the microsections a layer of a certain thickness was removed from the surface of weld made at each concentration of air in the protective nozzle, and not less than 10 measurements were taken in several regions of the microsection. Then the process was repeated, removing the metal layer with the measured hardness and hardness was measured again on the metal surface. Such a process was repeated until the values of weld metal hardness in the next layers practically did not change. For comparison, the same measurements were taken for the metal of welds made without air addition to the protective nozzle. The thus obtained data were used for plotting the following dependence: hardness of weld metal surface layer–distance from weld surface.

Content of gases (oxygen and nitrogen) was determined in the metal of welds at each concentration of air in the protective nozzle argon and without adding air to it. At assessment of the content of gases in the weld metal graphs were plotted by average values of the results for oxygen $[O]_{(Ar)}$ and nitrogen $[N]_{(Ar)}$ content in welds made in pure argon and welded at different concentrations of oxygen $[O]_{(Ar+air)}$ and nitrogen $[N]_{(Ar+air)}$ in the protective nozzle argon.

Mechanical testing of weld metal. To determine the ultimate strength and relative elongation of weld metal, samples for mechanical testing were cut out of the welds. A criterion for assessment of the properties of the metal of welds, made at addition of dosed air concentrations to argon, the values of ultimate strength and relative elongation in these welds were compared with the respective values of the metal of welds, produced at welding in argon without air addition. The results of mechanical testing and gas content in the metal of welds made without air addition in the protective nozzle, are given in work [7].

For static bend tests (10 mm width) samples were cut out across the weld, in keeping with Designation ASTM B265. Mandrel diameter D was selected from the condition $D = 5b$, where b is the sheet thickness ($b = 3$ mm). Before sample testing, grinding was used to remove the metal from the bead reverse side. Testing was followed by measuring the bend angle, as well as analyzing the weld surface for microcracks.

Investigation results. Oxygen presence in the arc gap was determined at the change of oxygen concentration in argon of the protective nozzle, in keeping with Table 1. As shown by investigations, despite an increase in oxygen content in argon of the protective nozzle (from 0.024 to 1.180 vol.%), no radiation of oxygen lines was found in the arc gap. It can be assumed that a certain part of the mixture of argon and air added to argon of the protective nozzle, is entrained due to injection by the peripheral part of the argon flow from the torch and is carried out without penetrating into the arc column. Another part is absorbed by the cooling solid surface of the forming weld and HAZ. It is also possible that part of oxygen molecules penetrates into the low-temperature regions of the arc, insufficiently dissociates and, that is why, no radiation of oxygen lines was registered in the arc.

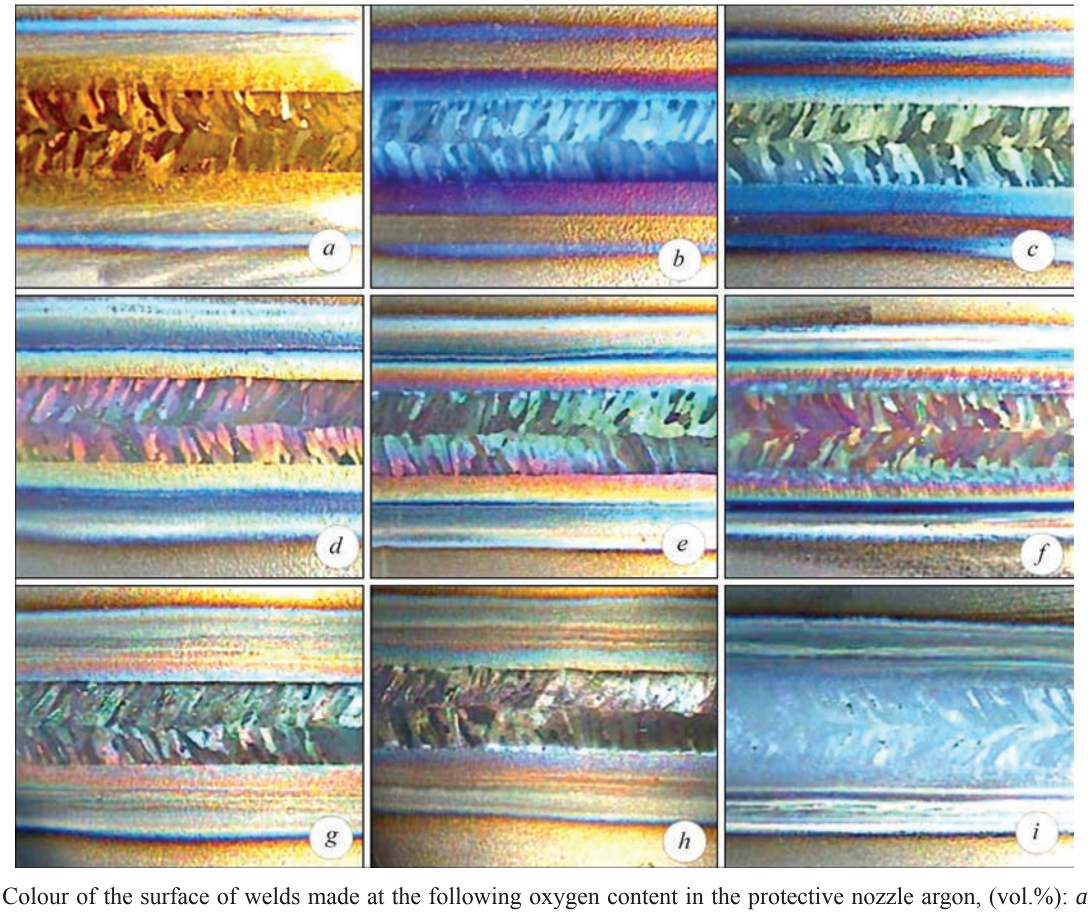

Figure 2. Colour of the surface of welds made at the following oxygen content in the protective nozzle argon, (vol.%): *a* — 0.024; *b* — 0.038; *c* — 0.074; *d* — 0.096; *e* — 0.120; *f* — 0.220; *g* — 0.320; *h* — 0.440; *i* — 1.180

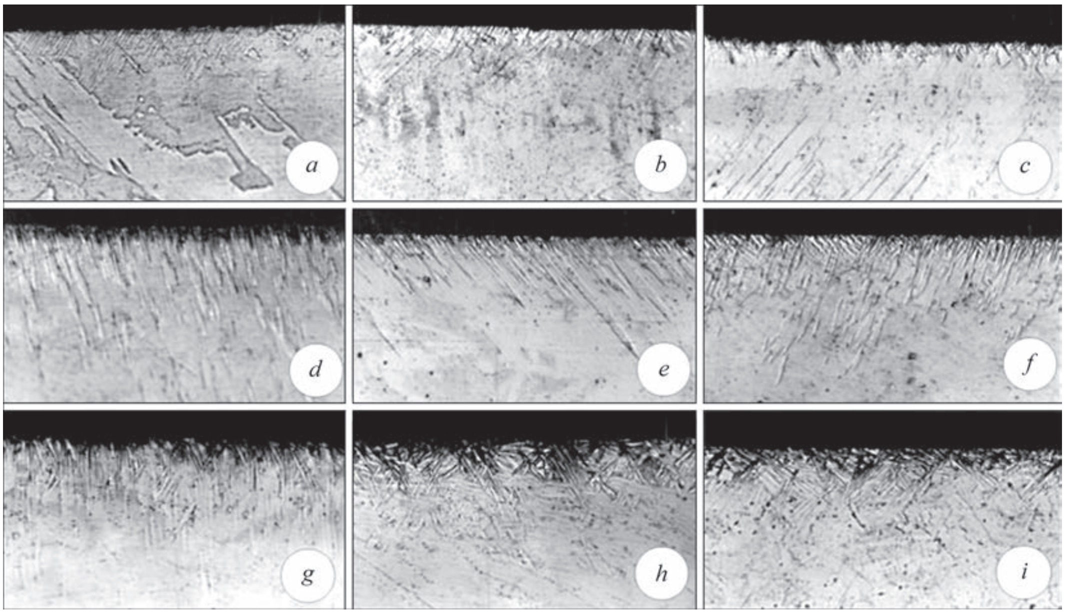

Figure 3. Microstructures (×250) of the surface layer of welds made at the following oxygen content in the protective nozzle argon (vol.%): *a* — 0.024; *b* — 0.038; *c* — 0.074; *d* — 0.096; *e* — 0.120; *f* — 0.220; *g* — 0.320; *h* — 0.440; *i* — 1.180

Analysis of the colour spectrum of the surface of weld metal led to the following conclusion. At increase of oxygen content in argon of the protective nozzle the weld surface colour changes from golden (0.024 vol.% oxygen) to grey-light blue (1.180 vol.% oxygen). Figure 2 shows the colours of weld surface, characteristic for each concentration value of air, which was added to the protective nozzle.

Microstructural analysis of surface layers of welds showed that at oxygen content of 0.024 vol.% in argon of the protective nozzle, a layer with thin acicular precipitates of not more than 0.012 mm depth forms on the weld metal surface (Figure 3, *a*). Such precipitates alternate with a structure typical for the metal of weld made in pure argon. At oxygen content of 0.038 vol.% in argon (Figure 3, *b*), a continuous layer with acicular structure of not more than 0.02 mm depth forms. Here, the needles have both the same and different direction relative to the surface. Such structural changes are associated with intensive absorption of oxygen and nitrogen in these regions of the metal. At further increase of oxygen content in argon up to 0.074 vol.% (Figure 3, *c*) the thickness of metal layer with an acicular structure also increases up to 0.05 mm. At 0.096 vol.% oxygen content in argon (Figure 3, *d*), the structure of the layer with an acicular morphology becomes inhomogeneous by the arrangement and size of the needles. Individual needles grow to the depth of 0.16 mm. Average depth of the layer is up to 0.07 mm. Further analysis of the microstructures shows that increase of oxygen content to 1.180 vol.% leads to increase of the depth of the layer with an acicular structure to 0.18–0.25 mm (Figure 3, *i*).

As a result of metallographic studies it was found that at air addition to the protective nozzle argon the surface layer of weld metal undergoes structural changes, associated with oxygen and nitrogen absorption. These changes occur to the depth of approximately 0.25 mm. No such structural changes were found in deeper lying regions of the weld.

The result of layer-by-layer measurement of weld metal microhardness for each value of oxygen concentration in the protective nozzle argon is shown in Figure 4. Comparison of the data given in Figures 3 and 4 leads to the conclusion that with increase of the quantity of air in the protective nozzle argon to 5.9 vol.% (1.18 vol.% oxygen) the depth of the metal surface layer with increased impurity content reaches approximately 0.20–0.25 mm.

Bending tests of the samples cut out across the weld without removing the surface layer, showed that bend angle is 180° for all the samples. It characterizes the metal as rather ductile. However, microcracks are found in the surface layer metal of all the samples (Figure 5).

Appearance of microcracks on the surface loaded by a tensile force, is attributable to low ductility of the metal surface layer, associated with increase of gas impurities in it. To assess the probable entrapment of air by the torch argon from protective nozzle argon and its absorption by weld pool metal, gas analysis of the weld metal was performed, and oxygen and nitrogen content was determined. Figure 6 gives the dependencies of the change of oxygen and nitrogen content in the welds on the concentration of these gases in the protective nozzle argon. Comparison of the obtained gas analysis results shows that with increase of air concentration in the protective nozzle argon, oxygen and nitrogen content in the weld metal stays practically within the same limits, as in welds, made in pure argon. These data lead to the conclusion that air addition to the protective nozzle argon within the studied limits does not increase the content of gases in welds. Therefore, it can be assumed that during welding the molten metal of the weld pool practically does not interact with oxygen and nitrogen of the air added to the protective nozzle argon.

To determine the influence of oxygen concentration in the protective nozzle argon on the strength and relative elongation of weld metal, flat samples were cut out for testing, locating them along the weld axis and removing 0.25 mm from the surface. Results of mechanical testing of the welds showed that despite an increased concentration of air in the protective nozzle argon in the studied range, the ultimate strength and relative elongation of weld metal (σ_t = = 456.9–451.4 MPa, β = 35.7–35.4 %) remain in the same ranges, as in welds, made in pure argon (σ_t = = 453.0 MPa, δ = 36.0 %).

Discussion of the results. Investigations showed that the colour of weld surface after welding depends on oxygen and nitrogen content in the protective nozzle argon. Results of investigations of the microstruc-

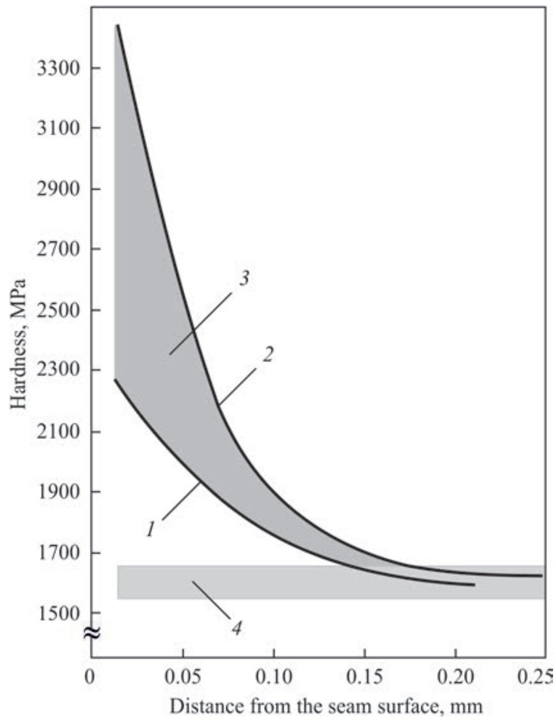

Figure 4. Microhardness of surface layers of the metal of welds made at the following oxygen content in the protective nozzle argon (vol.%): *1* — 0.024; *2* — 1.18; *3* — microhardness zone at oxygen content in the range of 0.038–0.440; *4* — zone of microhardness of the surface layer of a weld made without adding air to the protective nozzle argon

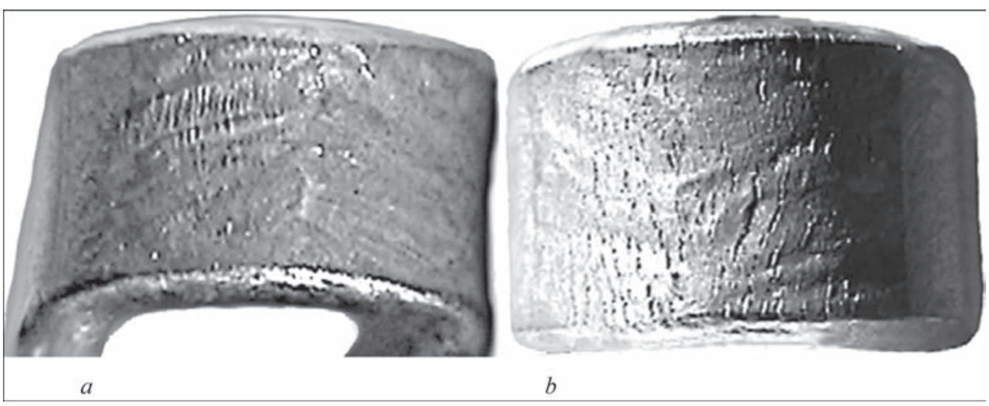

Figure 5. Microcracks on the surface of samples welded at the following oxygen content in the protective nozzle argon (vol.%): *a* — 0.024; *b* — 1.18

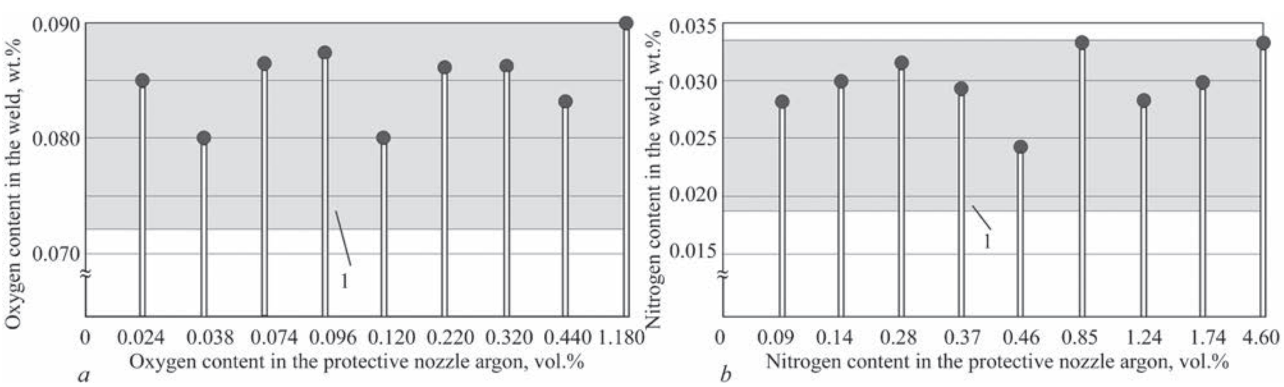

Figure 6. Content of oxygen (*a*) and nitrogen (*b*) in the welds, depending on the content of these gases in the protective nozzle argon: 1 — range of oxygen and nitrogen content in welds made without adding air to the protective nozzle argon

Table 2. Correlation dependence of weld surface colour–gas-saturated layer thickness–oxygen content in the protective nozzle

Weld index	Weld surface colour	Oxygen content in the protective nozzle argon, vol.%	Maximum thickness of a layer of higher hardness, mm
1		0.024	0.10
2	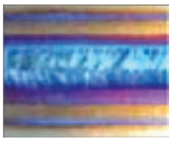	0.038	0.10
3	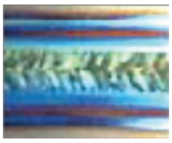	0.074	0.10
4	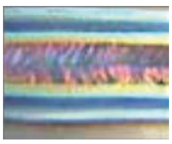	0.006	0.10
5	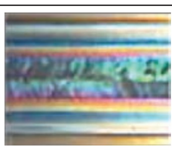	0.120	0.12
6	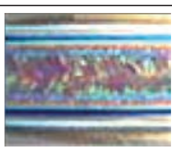	0.220	0.20
7		0.320	0.25
8		0.440	0.25
9	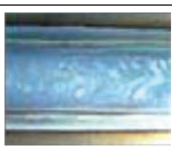	0.180	0.25

ture and layer-by-layer measurement of microhardness of the weld surface layer show a good matching of the data on the intensity of gas-saturated layer depth, depending on the weld surface colour. Thus, an experimental correlation was established between the change of weld surface colour and gas-saturated layer depth (Table 2).

Maximum depth of this layer is equal to not more than 0.25 mm. Investigations of bending test samples show that even at minimum content of oxygen in the protective nozzle argon (0.024 %) and golden colour of the weld surface (see Figure 2, *a*), microcracks form in it, which at the welded assembly operation under load can lead to its destruction, because of the surface layer brittleness.

Analysis of the results of gas analysis and mechanical testing of welds shows that oxygen and nitrogen of the air in the protective nozzle argon practically do not interact with the weld pool metal during welding. Therefore, in order to increase the operational reliability of welded structure assemblies with a coloured surface of a weld region, we can recommend removal of the gas-saturated layer to a depth, depending on weld colour, in keeping with the data in Table 2. If required, compensation of the removed metal by building-up is possible after removal of a layer, in keeping with the technological instructions.

1. Gurevich, S.M., Zamkov, V.N., Blashchuk, V.E. et al. (1986) *Metallurgy and technology of welding of titanium and its alloys*. 2nd Ed. Kiev, Naukova Dumka [in Russian].
2. Richardson, L.S., Grant, H.I. (1954) Reaction of oxygen and nitrogen with titanium from 700° to 1050°. *J. Metals*, **1**, 69–70.
3. Baj, A.S., Lajner, D.I., Slesareva, E.N., Tsypin, M.I. (1978) *Oxidation of titanium and its alloys*. Moscow, Metallurgiya [in Russian].
4. Mitra, T.K., Venkataraman, G. (1996). Effect of shielding on the properties titanium welds. *WRI J.*, 17(**4**), 117–121.
5. Mc Cue Don, Irving, B. (1999) Gas tungsten arc welding: It's built handle titanium. *Welding J.*, **11**, 31–36.
6. Dennis D. Harwig (1999) Achieving high-quality titanium arc welds. *Practical Welding Today (EWI Update)*, **1–2**, 48–50.
7. Prilutsky, V.P., Yeroshenko, L.E. (2021) Influence of conditions of welding pool protection by argon on properties of TIG of titanium. *The Paton Welding J.*, **6**, 39-43
8. *GOST R ISO 15614-5–2009*: Specification and qualification of welding procedures for metallic materials. Welding procedure test. Pt 5: Arc welding of titanium, zirconium and their alloys (Reedition) [in Russian].
9. Grabin, V.F. (1975) *Fundamentals of physical metallurgy and heat treatment of welded joints from titanium alloys*. Kiev, Naukova Dumka [in Russian].

Received 05.05.2021

https://doi.org/10.37434/tpwj2021.07.03

VACUUM BRAZING OF KOVAR–MOLYBDENUM DISSIMILAR JOINTS

S.V. Maksymova, P.V. Kovalchuk and **V.V. Voronov**
E.O. Paton Electric Welding Institute of the NAS of Ukraine
11 Kazymyr Malevych Str., 03150, Kyiv, Ukraine. E-mail: office@paton.kiev.ua

The features of spreading of brazing filler metals of Cu–Mn–Co system over molybdenum and Kovar were established based on the performed studies. Micro X-ray spectral analysis determined that zonal crystallization of a brazing filler metal drop on the base metal substrate occurs during spreading: pronounced areas of copper-based solid solution (Cu–12.92Mn–4.69Co) form along the outer perimeter of the drop, and dendrites of manganese-based solid solution, characterized by a higher melting point, are crystallized in the drop central part. It has been experimentally proven that an increase in the heating temperature contributes to an increase in the spreading area of the brazing filler metal by improving the spreading of copper-based solid solution. It was found that a copper-based solid solution forms in the brazed seam of dissimilar Kovar–molybdenum joints, and a molybdenum-based reaction layer (about 1 μm wide), crystallizes at the molybdenum-brazing filler metal interface. This layer is enriched in cobalt (15.80 %) and manganese (14.12 %) and contains a small amount of copper (1.63 %). As a result of mechanical tests of Kovar–molybdenum overlap joints under static loads at room temperature, destruction occurs partly along the brazed seam and partly along the base metal–molybdenum. 14 Ref., 2 Tables, 6 Figures.

Keywords: Kovar, molybdenum, vacuum brazing, dissimilar joints, copper-manganese-cobalt alloys, microstructure, strength, spreading

Individual components from dissimilar materials are often used to obtain certain properties of structures. Producing them by brazing involves a number of problems that is due to chemical composition of the materials being joined, and different physicomechanical properties.

At brazing dissimilar joints of molybdenum-stainless steel (Kovar), it is necessary to take into account the features of each material. Molybdenum belongs to refractory high-temperature materials due to a high melting temperature (2600 °C), and considerable specific strength under the conditions of high temperature. Its brazing is conducted under vacuum or in shielding gases, as it actively reacts with oxygen at heating in air that promotes its oxidation and lowers its mechanical properties [1]. Brazing temperature should not exceed its recrystallization temperature. At transition through recrystallization threshold, molybdenum becomes brittle [2] that is important to take into account at selection of the brazing filler metal and its melting ranges. Moreover, the difference in the coefficients of thermal expansion of both the metals leads to appearance of residual stresses, product deformations and crack initiation [3–5]. Therefore, at their combination copper and its alloys are usually used as brazing filler metal, which act as a damper between the parts being joined and promote relaxation of the arising stresses. Special ductile interlayers can be used, which are effective at joining dissimilar metals, with considerably different physicomechanical properties [4].

Much fewer works are devoted to joining molybdenum to Kovar (Fe–29Ni–17Co), compared to brazing molybdenum to stainless steel. Still, such work has been performed for many years, and it became particularly urgent in connection with development of new units and structural elements in instrument-making. At present, joining dissimilar Kovar–molybdenum materials, designed for high-temperature application, is urgent [5, 6]. Kovar belongs to precision alloys with specified temperature coefficient of linear expansion (TCLA), which is close to that of borosilicate glass [7] that promotes its application in optical instruments operated in a broad temperature range. Brazing of these metals involves problems of a different nature. On the one hand, their TCLA are close: for Kovar it is equal to ~ $4.6–5.29\cdot10^{-6}$ °C^{-1} (in the temperature range of 20–400 °C and it grows rapidly with increasing temperature) [8], and for molybdenum it is equal to $5\cdot10^{-6}$ °C^{-1} (in the temperature range of 0–100 °C) that is a positive moment when making Kovar–molybdenum brazed joints. On the other hand, however, based on melting diagram of Mo–Fe system one can see that molybdenum and iron have considerable areas of solubility at high temperature. With its

S.V. Maksymova — https://orsid.org/0000-0003-0158-5760, P.V. Kovalchuk — https://orsid.org/0000-0002-2313-5982,
V.V. Voronov — https://orsid.org/0000-0002-0410-1154

Table 1. Chemical composition of experimental materials, wt.%

Composition	Fe	C	Si	Ni	Co	Mo
Mo	Up to 0.01	Up to 0.005	Up to 0.01	Up to 0.005	–	min 99.96
29NK	51.14–54.5	–	–	28.5–29.5	17.0–18.0	–

lowering, however, these areas rapidly become narrower and at room temperature the mutual solubility is practically absent. A series of intermetallic phases forms between the considered elements, which can have a negative role, leading to brittleness of the brazed joint [9]. Formation of intermetallic phases has a negative influence on the mechanical properties of dissimilar joints, which were produced by different methods, also by welding [6, 10]. Detailed studies of microstructure of the joints produced at electron beam braze-welding of Kovar with molybdenum showed that three zones form on the joint interphase, where an iron-based and molybdenum-based solid solutions were found, as well as brittle intermetallic phases: Fe_5Mo_3, FeMo, which are the cause of brittle fracture and low strength [10].

At vacuum brazing of Kovar to molybdenum (at the temperature of 1115 °C), using pure copper 100 μm thick as brazing filler metal, the joint strength is equal to 72–75 MPa [5].

This work presents the results of investigations on spreading of experimental brazing filler metals of Cu–Mn–Co system on Kovar and molybdenum and features of formation of the structure of dissimilar Kovar–molybdenum brazed joints that were produced by vacuum high-temperature brazing.

Experimental part. Molybdenum sheets of MCh grade (3 mm thick) and Kovar precision alloy (2 mm thick, Table 1) were used as base metal to conduct the experiments.

Experimental brazing filler metals were produced on a copper backing in an argon atmosphere with application of arc heating. In order to study the influence of cobalt on solidus and liquidus temperature, a number of experimental alloys of Cu–Mn–(0.5–4.5)Co system were produced and their melting ranges were determined by high-temperature differential thermal analysis (HTDTA) (Table 2), using VDTA-8M3 unit in high-purity helium at the heating rate of 40 °C/min (±5 °C).

In order to conduct the experiments, Cu–Mn–(0.5–4.5)Co polycrystalline alloys in the cast and rolled state were used in the form of a strip of ~ 100 μm thickness.

Experiments on spreading of the studied alloys were conducted on molybdenum substrates of 15×15 mm size. Brazing filler metals in the quantity of 300 mg were placed in the central zone of base metal substrate, heating was conducted in a vacuum furnace with radiation heating at the temperature that exceeds the liquidus temperature by 30 °C at rarefaction of the working space of $1.33 \cdot 10^{-4}$ Pa for 180 s. The spreading areas of experimental brazing filler metals were measured using scanning and KOMPAS-3Dv17.1 program.

Brazing dissimilar overlap joints (with a capillary gap) was also performed at the temperature which exceeds T_L by 30 °C, soaking time was 180 s. Obtained samples were cut normal to the sheet surface and microsections were prepared by a standard procedure and their chemical heterogeneity was studied, using a scanning electron microscope TescanMira with LMU. Micro X-ray spectral studies and determination of local distribution of elements in individual phases were conducted using energy-dispersive spectrometer Oxford Instruments X-max 80 mm^2, which is fitted with INCA program package. Microsections were studied without chemical etching.

Experimental results and their analysis. Obtained investigation results showed that experimental alloys have a quite narrow melting range, not exceeding 22–35 °C, but increasing cobalt concentration leads to its widening due to increase of liquidus temperature. With increase of cobalt concentration from 0.5 to 4.5 wt.%, the alloy solidus temperature rises by 14 °C.

When conducting the experiments, the maximum overheating above the alloy solidus temperature was equal to 65 °C (Figure 1).

Ternary alloys of Cu–Mn–(0.5–4.5)Co system are characterized by a cast structure that is formed by two solid solutions based on copper and on manganese. The latter is observed in the form of dark dendrites of the solid solution with pronounced liquation by the

Table 2. Experimental alloys and temperature of spreading (brazing)

Alloy number	Composition, wt.%	Spreading temperature, °C	Melting temperature range, °C	Heating above solidus temperature, °C
1	Cu–Mn–0.5Co	939	22	52
2	Cu–Mn–1Co	946	21	51
3	Cu–Mn–2Co	955	26	56
4	Cu–Mn–4.5Co	966	35	65

component elements that is inherent in alloys of this system [11]. Cobalt is a component element of both the solid solutions. Kovar structure is single-phase and is formed by γ-solid solution, which is resistant at the temperature higher than –70 °C. At an unfavourable ratio of nickel and cobalt and present impurities, partial $\gamma \rightarrow \alpha$ transformation (of martensite nature) is possible at T = –70 °C, which may lead to TCLA increase that should be taken into account at creation of structures and components from such dissimilar materials as Kovar and molybdenum.

It is known that one of the important physicochemical characteristics of producing a sound joint is the ability of brazing filler metal to wet the base metal and spread over it [12]. The quality of brazed products depends on the completeness of running of this complex metallurgical process. Proceeding from the conducted investigations, it was found that at spreading of cast brazing filler metal (Figure 2, *a*) of Cu–Mn–CO system on molybdenum, a drop of inhomogeneous structure forms, which can be conditionally divided into zones (Figure 2, *b*, *c*).

In the central zone (No.1), a manganese-based solid solution crystallizes as dispersed dendrites, which form the tip of brazing filler metal drop. They are located against the background of the copper matrix, but their liquidus temperature is higher than that of copper-based solid solution [13]. The results of micro X-ray spectral analysis revealed considerable chemical inhomogeneity of the intermediate zone (No.2) which is a copper-based solid solution of varying concentration. The morphology of this zone differs considerably from the previous one, and consists of rather coarse dendrites of the solid solution with a pronounced liquation by component elements (Figure 2, *d*) that is determined by the cooling rate and crystallization temperature range [11]. Manganese concentration is in the range of 16.2–32.15 %.

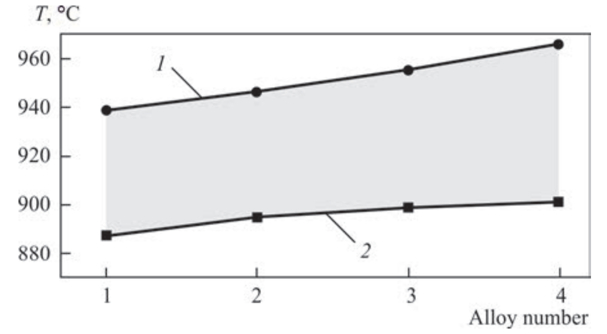

Figure 1. Brazing temperature (*1*) and solidus temperature (*2*) of experimental alloys

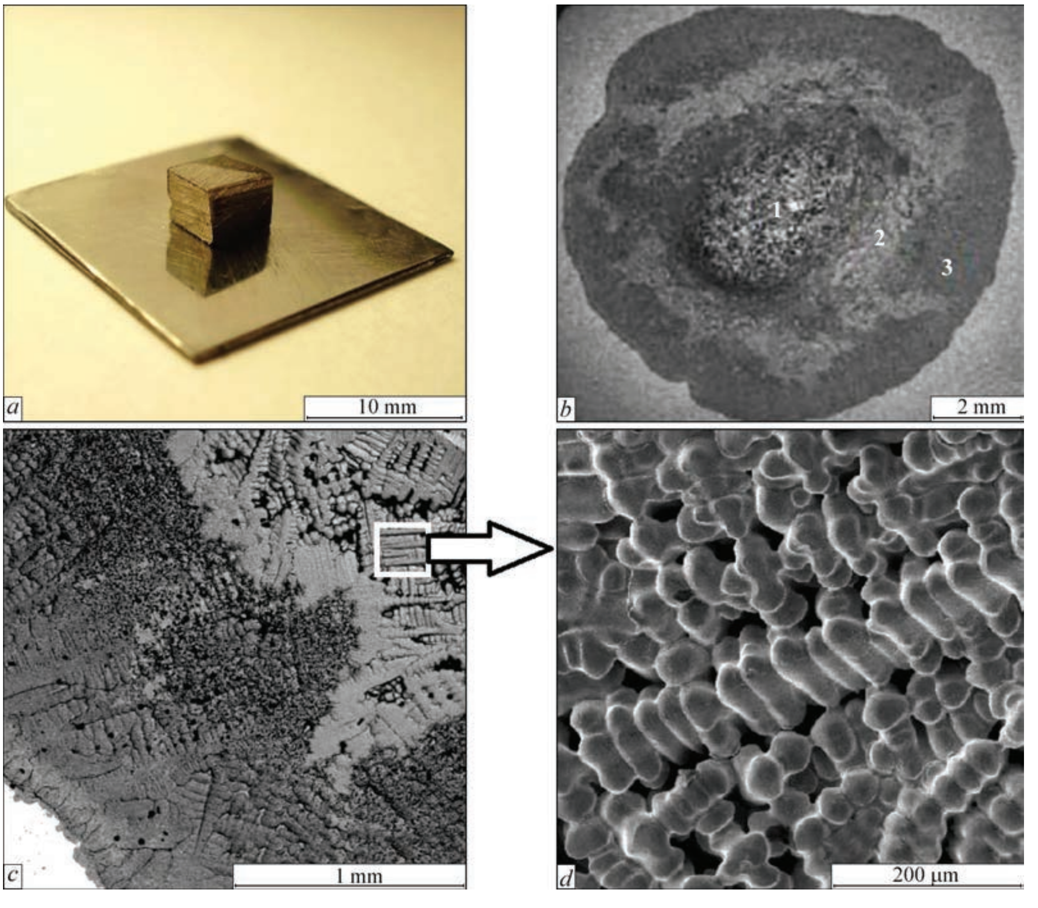

Figure 2. Cu–Mn–4.5Co brazing filler metal on a molybdenum substrate (*a*), after spreading (*b*, *c*) and structure of the intermediate zone – dendrites of copper-based solid solution (*d*)

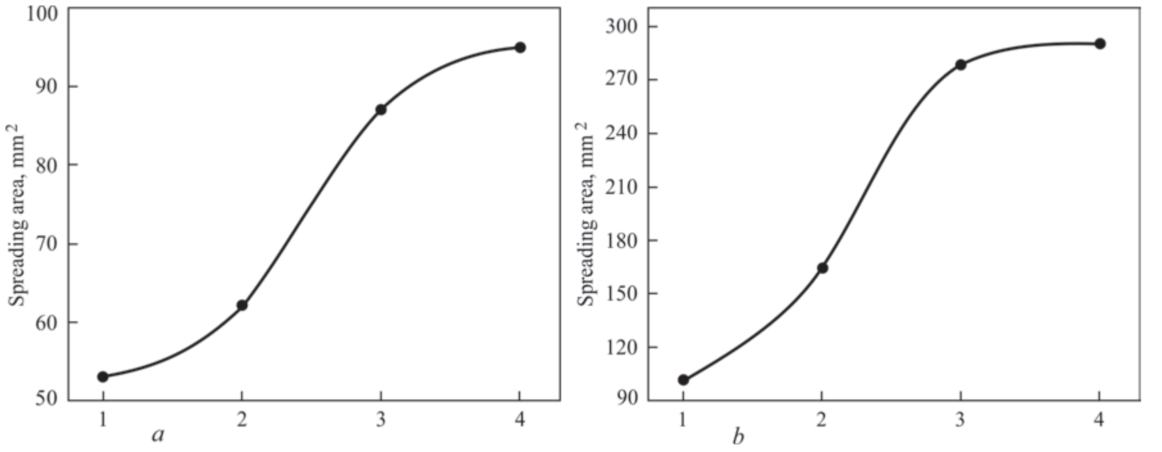

Figure 3. Spreading area of brazing filler metals Nos 1–4 of Cu–Mn–Co system, on molybdenum (*a*) and on Kovar (*b*)

A halo in the form of a plane crystallization front is observed around the drop perimeter (zone No.3), which is formed by a copper-based solid solution with minimum manganese concentration (12.92Mn), which is characterized by the lowest melting temperature and is the last to crystallize. The low concentration of manganese in this zone is due to high vapour pressure and time of brazing filler metal staying in the liquid state under vacuum. Note that zonal formation of the structure at molybdenum spreading is characteristic for all the studied brazing filler metals (see Table 1).

It was proved experimentally that at increase of heating temperature the area of brazing filler metal spreading increases (Figure 3, *a*) due to improvement of spreading of copper-based solid solution, which crystallizes around the perimeter of brazing filler metal drop in the form of a halo. The tendency to increase of the area is observed at spreading of experimental brazing filler metals both on molybdenum (Figure 3, *a*), and over Kovar (Figure 3, *b*). Obtained data show the good capillary properties of brazing filler metals of Cu–Mn–Co system.

Dissimilar reference-samples were brazed simultaneously with samples for mechanical testing, in order to study the brazed seam properties and conduct metallographic examination. External examination of the samples showed that at brazing of dissimilar molybdenum-Kovar joints (by Cu–Mn–4.5Co brazing filler metal) formation of a full direct and reverse fillet section is observed (Figure 4, *a*, *b*).

Micro X-ray spectral analysis showed that the brazed seam metal consists of a matrix — copper-based solid solution of Cu–Mn–Ni, which contains 2.87 % cobalt and 3.73 % iron. A molybdenum-based reaction layer (about 1 μm wide), enriched in cobalt (15.80 %), and manganese (14.12 %) and having a small amount of copper (1.63%), forms on molybdenum–brazing filler metal interphase.

Moreover, a small amount of discrete grains based on iron (27.05–28.29 %) and enriched in manganese (27.94–26.93 %) is observed against the background of the solid solution that is confirmed by investigations at electron beam scanning of the brazed sample (Figure 5).

Note that such features of structure formation are due to nonequilibrium conditions of crystallization of brazed seam metal, presence of concentration gradient on base metal – brazing filler metal interphase and diffusion processes running during brazing. Owing to

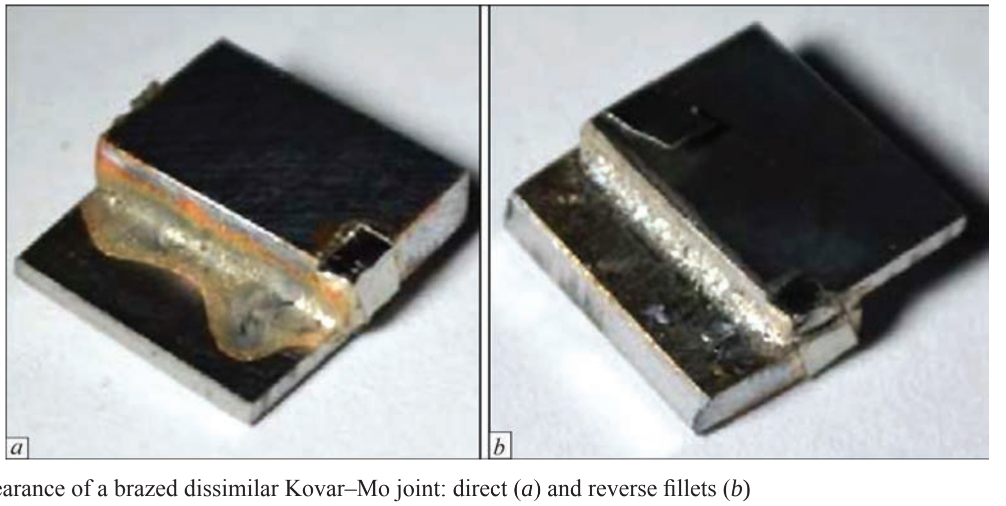

Figure 4. Appearance of a brazed dissimilar Kovar–Mo joint: direct (*a*) and reverse fillets (*b*)

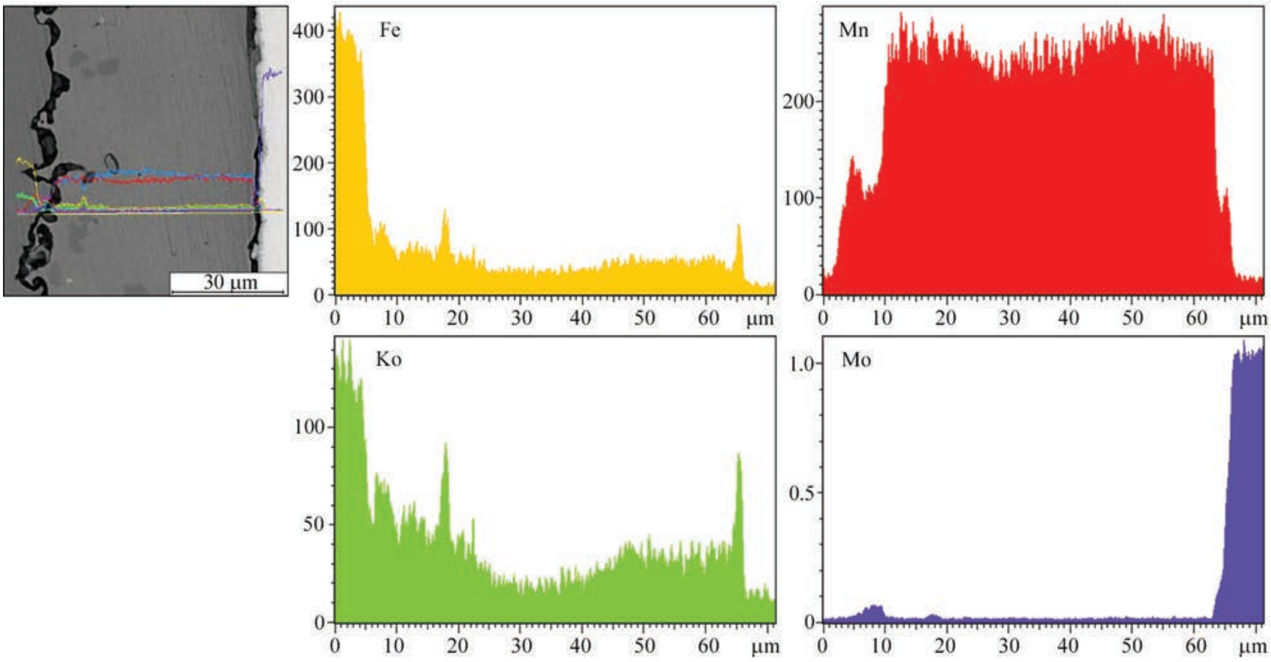

Figure 5. Electron image and distribution of iron, manganese, cobalt, and molybdenum in the weld of brazed dissimilar Kovar–Mo joint

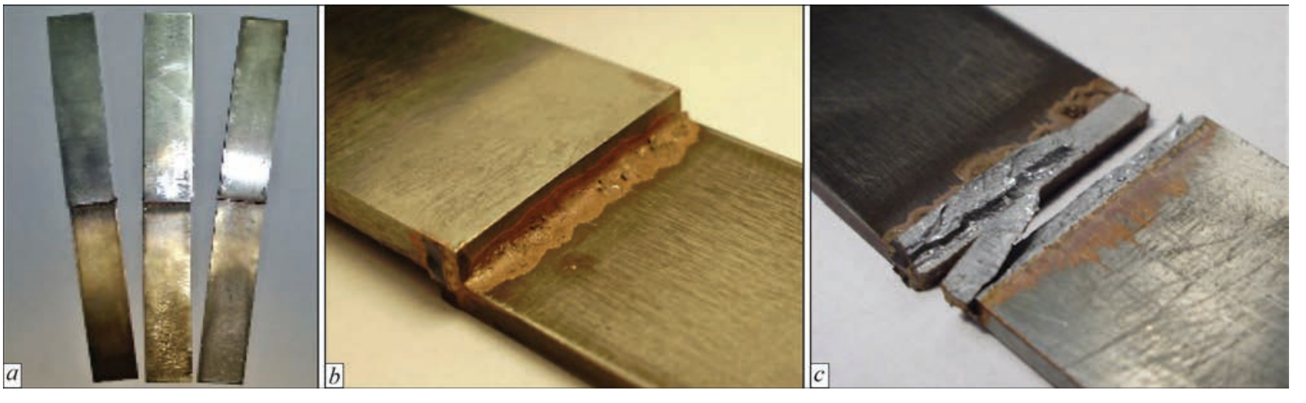

Figure 6. Appearance of brazed Kovar–molybdenum samples before (*a*, *b*) and after testing (*c*)

diffusion processes, the brazed seam meal is saturated by base metal elements, and, as a result, it differs from the initial brazing filler metal by chemical composition, that affects the mechanical properties of the brazed joints.

Overlap sheet brazed Kovar–molybdenum samples were used to study the mechanical properties under static loading conditions at room temperature [14] which were produced with application of brazing filler metal (No.4) Cu–Mn–4.5Co. Their appearance in the initial condition (as-brazed) is indicative of sound formation of the fillet sections and absence of pores in the welds (Figure 6, *a*, *b*).

During testing destruction of the samples occurs partially in the brazed seam and partially in the base metal–molybdenum (Figure 6, *c*). Proceeding from mechanical testing results, it was determined that the shear strength of brazed Kovar–molybdenum samples is in the range of 168.18– 278.87 MPa.

Conclusions

Obtained investigation results showed that at spreading of brazing filler metals of Cu–Mn–4.5Co system on molybdenum, zonal crystallization of brazing filler metal drop takes place. Pronounced regions with plane fronts of crystallization of copper-based solid solution (Cu12.92Mn–4.69Co) form around the drop perimeter. In the intermediate zone, dendrites of copper-based solid solution, containing a varying concentration of manganese (16.2–32.15 %) are observed that is due to dendritic segregation at crystallization.

Dendrites of manganese-based solid solution form in the drop central (upper) zone against the background of copper-based solid solution. Their melting temperature is higher than that of copper-based solid solution.

It is found that increase of the heating temperature leads to increase of brazing filler metal spreading area that is due to melting temperature of copper-based solid solution which practically does not change.

Shear strength at room temperature of brazed overlap dissimilar Kovar–molybdenum samples is in the range of 168.18–178.87 MPa. Destruction of the samples runs partially through the brazed seam and partially–through base metal–molybdenum.

1. Tits, T., Wilson, J. (1969) *Refractory metals and alloys*. Ed. by P.K. Novikova, I.I. Novikov. Moscow, Metallurgiya [in Russian].
2. Gurevich, S.M., Nerodenko, M.M., Kharchenko, G.K. et al. (1982) *Metallurgy and technology of welding of refractory metals and alloys on their base*. Kiev, Naukova Dumka [in Russian].
3. Yermolayev, H.V., Kvasnytskyi, V.V., Kvasnytskyi, V.F. et al. (2015) *Brazing of materials:* Manual. Ed. by V.F. Khorunov, V.F.,Kvasnytskyi. Mykolaiv, NUK [in Ukrainian].
4. Liu, G.W., Valenza, F., Muolo, M.L. et al. (2010) SiC/SiC and SiC/Kovar joining by Ni–Si and Mo interlayers. *J. Mater. Sci.*, 45, 4299–4307. DOI: https://doi.org/10.1007/s10853-010-4337-3
5. Kumar, S., Upadhyay, A., Dinesh Kumar, P., Agarwal, A. (2015) *Vacuum brazing of molybdenum–Kovar and evaluation of its joint strength*. MSF 830–831, 282–285. DOI: https://doi.org/10.4028/www.scientific.net/msf.830-831.282
6. Chen, G., Yin, Q., Guo, C. et al. (2019) Beam deflection effects on the microstructure and defect creation on electron beam welding of molybdenum to Kovar. *J. Materials Proc. Technology*, 267, 280–288. DOI: https://doi.org/10.1016/j.jmatprotec.2018.12.017
7. (1983) *Precision alloys:* Refer. Book. Ed. by B.V. Molotilov. 2nd Ed. Moscow, Metallurgiya [in Russian].
8. Buturlya, E.A., Bugaenko, B.V., Petrenko, L.M., Golub, D.M. (2019) Features of active brazing of ceramics with metals. *Visnyk DDMA*, 45(**1**), 38–42 [in Ukrainian].
9. (1997) *State diagrams of binary metal systems:* Refer. Book. Ed. by N.P. Lyakishev. In: 3 Vol., Vol. 2. Moscow, Mashinostroenie [in Russian].
10. Chen, G., Yin, Q., Dong, Z. et al. (2020) Microstructure evolution analysis for the reaction interface between molybdenum and Kovar acquired by electron beam welding-brazing. *Materials Characterization*, 171. DOI: https://doi.org/10.1016/j.matchar.2020.110781
11. Favstov, Yu.K., Shulga, Yu.N., Rakhshtadt, A.G. (1980) *Metals science of high-damping alloys*. Moscow, Metallurgiya [in Russian].
12. Krasovskyi, V.P., Gab, I.I., Stetsyuk, T.V., Krasovska, N.O. (2017) Wetting of quartz glass by low-melting brazing melts. *Adgeziya Rasplavov i Pajka Materialov*, **50**, 18–27 [in Russian].
13. Drits, M.E. (1979) *Binary and multicomponent copper-based systems:* Refer. book. Moscow, Nauka [in Russian].
14. Maksymova, S.V., Kovalchuk, P.V., Voronov, V.V. (2019) Influence of cobalt on structure and technological properties of Cu-Mn system alloys. *Metalofiz. Novitni Tekhnologii*, 41(**10**), 1365–135. DOI: https://doi.org/10.15407/mfint.41.10.1365

Received 26.05.2021

https://doi.org/10.37434/tpwj2021.07.04

HEAT-PULSE WELDING OF WOVEN POLYMERIC SHEET MATERIALS

M.G. Korab, M.V. Iurzhenko, A.V. Vashchuk and **A.M. Galchun**
E.O. Paton Electric Welding Institute of the NAS of Ukraine
11 Kazymyr Malevych Str., 03150, Kyiv, Ukraine. E-mail: office@paton.kiev.ua

The aim of the work is to test the technology of welding filter bags made of polyester ultralight fabric of linen weaving. The tasks are the choice of welding method, creating an experimental installation, adjusting the parameters of the welding process and evaluating the quality of the produced welds. The method of heat-pulse welding with T-shaped welt seams with continuous penetration and simultaneous cutting of the welded material was chosen. An experimental installation with a heating element made of nichrome wire of 0.8 mm diameter was developed. During one cycle of heat-pulse welding, two longitudinal welds, the so-called T-shaped welt seams are formed, the shape and size of which depend on the heating mode of the polymeric material. Welded filter bags were turned before using in such a way that T-shaped seams in the working environment were directed inwards and the load on dangerous areas of welds was reduced. Mechanical tests of welds of filter polyester fabric produced by heat-pulse welding showed a sufficient level of their mechanical strength. To control the quality of the finished filter bags, it is sufficient to visually inspect the welds for leaks or other obvious defects. Results of the work is the technology of manufacturing filter bags from mesh polyester fabric by means of heat-pulse welding of welt seams with continuous penetration and cutting of the welded material is worked out. The welding installation was created. Parameters of a welding mode were established. It was determined that produced welded joints in terms of strength characteristics meet the necessary criteria for the intended use of filter bags made of ultra-thin polymeric fabrics. 9 Ref., 8 Figures.

Keywords: thermoplastics, welded joints, polyester fabric, heat-pulse welding

Polymers are used as construction materials in different fields of production [1–3]. In particular, fabrics made of polyester synthetic fibers are widely used both in the production of consumer goods as well as in different technical products. The most well-known representative of polyesters used for the production of fibers is polyethylene terephthalate (PET). The traditional name for PET in post-Soviet countries is lavsan, other trade names for this polymer are dacron (USA), terylene (Britain), tekadur (Germany), and tetoron (Japan). PET is an aliphatic-aromatic polyester obtained by polycondensation of ethylene glycol with teraphthalic acid. This polymer is a solid rigid thermoplastic, transparent in the amorphous state and white in the crystalline state.

The production of polyester fiber is carried out by the traditional method of extrusion, i.e. by squeezing a melt of polyethylene terephthalate through numerous ultra-thin holes in the die with the following air cooling. For the production of yarn (threads) in the textile industry, so-called staple fibers of a specially determined length, not more than 40–45 mm, are used [4]. The vast majority of all synthetic threads of different types are used for the production of different fabrics.

The principle of fabric production has remained unchanged for many centuries. Technical filter fabrics, depending on the field of application differ in the method and density of weaving. In the modern textile industry, dozens of different types of weaving are used, the simplest of which is linen, when longitudinal threads (warp) and transverse threads (weft) alternately intersect. The geometric density of fabric is determined as a number of threads per unit length [5].

An important area for application of technical polyester fabrics is filter elements for laboratory equipment designed to determine the specific content of cellulose (non-nutritious part) in plant products. Determination of cellulose content by the Weende method consists in the fact that the sample of plant product is first subjected to hydrolysis in a solution of sulfuric acid, and then to alkaline hydrolysis in a solution of sodium hydroxide [6]. Samples of products during laboratory analysis are loaded into special small bags of filter fabric. At the present, such packages are not produced in Ukraine, though they are in a great need. Therefore, the development of domestic technologies and equipment for production of filter bags is an urgent task. For joining fabrics of polymeric thermoplastic fibers, it is possible to use those welding methods which are developed for polymeric films [7, 8].

For production of filter bags, polyester ultralight technical fabric of linen weaving of the Saatifil brand was chosen [9]. The fabric of the article PES 68/38 is

M.G. Korab — http://orcid.org/0000-0001-8030-1468, M M.V. Iurzhenko — http://orcid.org/0000-0002-5535-731X,
A.V. Vashchuk — http://orcid.org/0000-0002-4524-4311

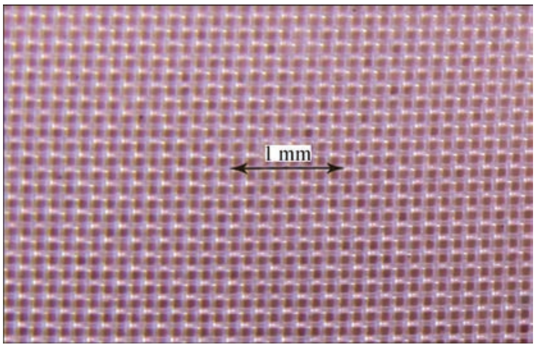

Figure 1. Structure of light polyester (lavsan) filter fabric of linen weaving

resistant to the action of acids and alkalis at elevated temperature, it has a milky color and its specific weight is 32 g/m^2.

Figure 1 shows an enlarged view of the structure of the polyester fabric PES 68/38. Linen weaving of a low-density provides the formation of a mesh structure of the fabric uniform in both directions and well permeable to air and water. The linear density of the fabric amounts to 90 threads per centimeter. The longitudinal and transverse threads of the fabric are absolutely identical, the average diameter of the thread, which consists of several polyester monofibers, is 40 μm. The average size of the square gaps between the threads is 68 μm. Therefore, during the research works the fabric can reliably hold fragments of a refined material with a minimum size of 0.1 mm.

A filter bag of polyester fabric is 120 by 45 mm in size. Its production according to the standard technology of sewing with threads is difficult and low-efficient. There is a technology of welding filter bags by ultrasonic method, according to which by means of the inlet weld, from the band a fabric sleeve is formed, and in the second stage a «bottom» is formed by the transverse T-shaped weld. However, the strength of such welds is not more than 35–40 % from the level of the base material, which leads to their frequent fractures during the analysis. A promising method of joining ultra-thin thermoplastic material in the manufacture of filter bags is heat-pulse welding using a heated tool.

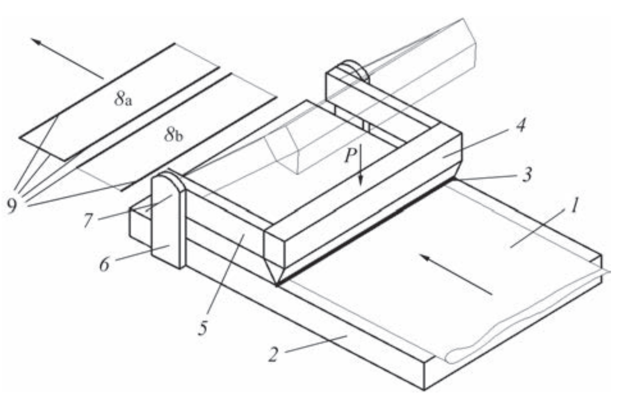

Figure 2. Schematic diagram of experimental installation for heat-pulse welding of filter bags (designation see in the text)

Welding of ultra-thin polymeric materials with a thickness of up to 250 μm, which are very sensitive to excessive heating of material in the joint area, is performed by heat-pulse method using a heating tool of low weight and heat capacity, which is heated for a short time by a powerful electric pulse. In this case, the method of heat-pulse welding by T-shaped welt seams with full penetration and simultaneous cutting of the welded material was chosen.

To optimize the process operation diagram of welding thin polyester fabric, an experimental installation was designed (Figure 2). On a rectangular base *2* all parts of the installation are fixed and welded materials *1* are placed. The wire heating element *3* is fixed in the lower part of the housing of the upper electrode *4*. From the rear side, two brackets *5* are attached to the electrode, connected by their ends to the vertical struts *6* by a horizontal axis *7*. The upper electrode with the brackets can swing relative to the axis *7*, getting into contact with the base plane, its own weight is sufficient to create a working force of pressing *P*. The heating element was made of cylindrical nichrome wire of 0.8 mm diameter and 150 mm length. The heater through the insulating gasket was fixed in the lower part of the movable electrode of the installation with the connection of the power supply wires.

Two process operation diagrams of filter bag formation were compared. In the first variant, two samples of fabric were welded laid on each other and filter bags of type 8a with two side and one lower weld were obtained. In the second variant, the samples of fabric were welded, folded in half in the longitudinal direction, and bags of type 8b were welded with two side welds and a bottom, formed by the fabric fold, were obtained.

When through the heating element electric current of 9–10 A passes, the wire is heated to the saturation temperature at the level of 270–290 °C for about 1 s and then its temperature increases slowly. Therefore, heating of the welding zone was regulated by the duration of the operating current pulse.

The stages of the process of heat-pulse welding of polyester fabric are schematically shown in Figure 3. At the initial stage (Figure 3, *a*) the heating element *1* approaches the place of welded joint of fabric samples *2*, which are laid in two layers on a flat base *3*. After that, the power source is turned on and the working current pulse begins. At the second stage (Figure 3, *b*), the heated wire tool begins to melt a polymeric material of the fabric. Under the action of the pressing force, the heating tool is gradually lowered, melting first the upper layer of the fabric and then the lower one. Such melting is finished at the moment, when the heater touches the surface of the base and both layers of the fabric are cut with a cylindrical wire at the place of joining. On both sides

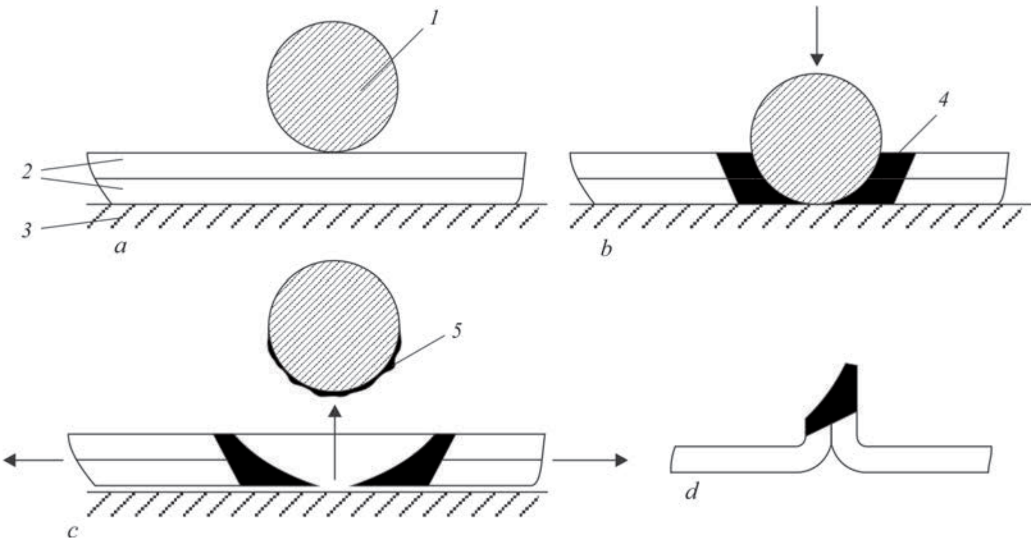

Figure 3. Main stages of technological process of heat-pulse welding with simultaneous thermal cutting (designation see in the text)

of the heater, small volumes of a molten polymer 4 are formed, which subsequently form welds.

Thus, in one cycle of heat-pulse welding, two longitudinal welds are formed on both sides of the cylindrical heating element. After a complete penetration of the fabric, its cut parts are removed from each other (Figure 3, c), the heating element is raised and removed from the welding zone. On the surface of the heater wire, a small amount of molten polymer material 5 remains. If the duration of a working current pulse is extended by 1–2 s, the stickened material completely evaporates and has almost no effect on the quality of the weld to be produce in the next cycle. The developed technology allows producing so-called T-shaped welt seams, the shape and size of which depend on the heating mode of the polymeric material. Usually in a working condition such seams are located perpendicularly to the main plane of fabric (Figure 3, *d*).

Tests of welded bags under the conditions simulating workloads showed that from the point of view of fracturing, the most dangerous are the initial areas of the welds near the neck of the small bag and the final areas of the welds at the corners of a product. Therefore, it was decided to turn out filter bags before using so that the welts of T-shaped seams in the working environment were directed inwards. The load on the dangerous areas of the welds in this case is significantly reduced due to changes in the geometric shape of the fabric (Figure 4).

The T-shaped welt seam of polyester fabric is formed as a result of melting the sewn polymer material of the fabric, which after cooling and hardening forms a solid rigid polymer structure. As a result, a welded joint of a flexible mesh fabric linen is formed, consisting of a fibrous material with a solid hardened polymeric material of the weld (Figure 5). During loading of a T-shaped welt seam, the main stresses are concentrated in a narrow zone along the weld, where the fibrous sewn material of the fabric mates the hardened rigid polymeric material of a weld. Therefore, the size and shape of the weld itself have little effect on the strength of welded joint.

The mesh fibrous polymeric material of the filter fabric melts rather quickly at a temperature of 260–270 °C. Therefore even at a short contact of a heater with a fabric, within 3–5 s, on a fabric the longitudinal band of 1–2 mm width melts. As a result, after hardening of the melt, a solid polyester welt with a width from 1 to 3 mm is formed having a nonuniformly distributed thickness along the weld. Moreover, the welded joint itself at the place of contact between fabric threads and a solid weld has almost the same thickness, which is approximately equal to the thickness of one layer of the filter fabric. This is clearly seen in the enlarged image of the cross-section of the weld (Figure 5).

To evaluate the strength parameters of T-shaped welds of polyester fabric, a series of mechanical tests

Figure 4. Turned out filter bag prepared for use

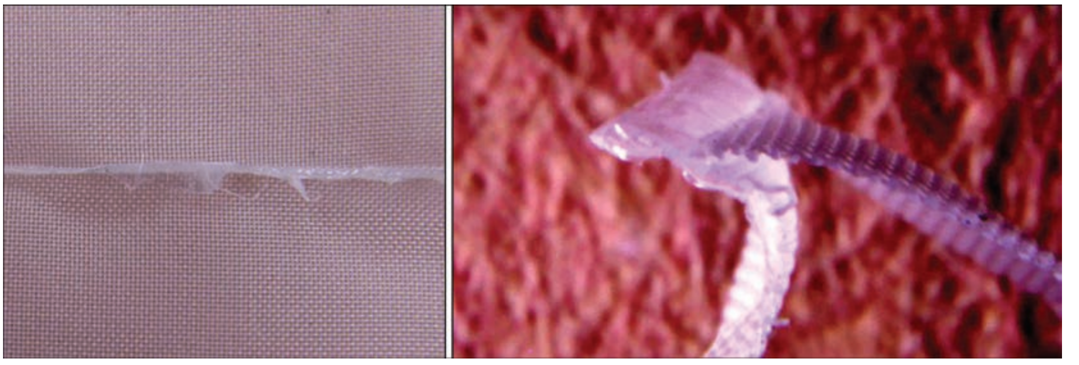

Figure 5. Longitudinal T-shaped weld of polyester filter fabric

were performed. The strength of welded joints of the fabric was determined with the use of a rupture machine during tensile tests of band samples of 50 mm width with a welt seam in the center of the sample. With the excess in the critical load level, the fracture of the weld begins in the weakest places on both sides from a rigid welt formation, and the hardened polymeric material of the weld remains sound. When tearing away the main linen from the weld, the mesh structure of a linen weave of the fabric maintains its regularity and remains almost sound. Thus, the main factors influencing the strength of welded joint of a filter fabric are physical and geometric parameters of the place of joining each transverse thread of the fabric relative to the weld with a rigid polymeric material of a T-shaped welt. Thus, the strength of the entire weld is formed as an integral sum of the strength of attachment of individual threads to the monolithic material.

A linen mesh weaving of fabric with a small density of threads adjacent to each other creates a symmetrical spatial structure of the fabric without significant differences between the shape of longitudinal and transverse threads. All threads of the fabric after weaving acquire a wavy sinusoidal shape. Therefore, in the area of joining the fabric with the weld, there are alternating «upper» and «lower» transverse threads, intertwined relative to the longitudinal thread. Accordingly, flattenings on the threads near the joint are formed alternately either from top, or from bottom, which in the photos of the weld in the plan looks like alternation of such formations through one (Figure 6).

During fracture of the seam of the fabric under the action of tensile load, the rupture occurs along the line of joning, which is formed by a chain of flattened transverse threads, partially joined with remnants of a longitudinal thread, which is not completely melted during welding. Along the fragment of the fabric edge torn from the weld, deformed ends of the upper and lower transverse threads alternately follow one another. At the enlarged image of the torn edge (Figure 7), it is seen that deformation of the ends of the threads represents namely flattening of a fibrous cylindrical material, which becomes flat, expands and reduces its thickness.

The scheme of forming a welded joint of a mesh thread structure, inherent to polyester fabric, is presented in Figure 8. Fragments of the fabric to be joined are formed by interweaving of transverse and longitudinal threads relative to the weld line. In the process of welding, a part of threads, which directly undergo the action of the heating tool, melts and forms a solid array of a polymer melt along the entire weld line. Since the process of heating the weld is short and takes units of seconds, threads that do not have a direct contact with the heater, are almost not subjected to thermal effect and do not change their size and shape. This applies to the threads longitudinal relative to the weld, which in the mesh fabric are separated by free gaps of 65–70 μm. Longitudinal threads directly adjacent to the fusion line are melted only partially and in selected areas depending on their distance to the heater during welding.

On the contrary, all transverse threads inevitably contact with the heating tool during heating of the wo-

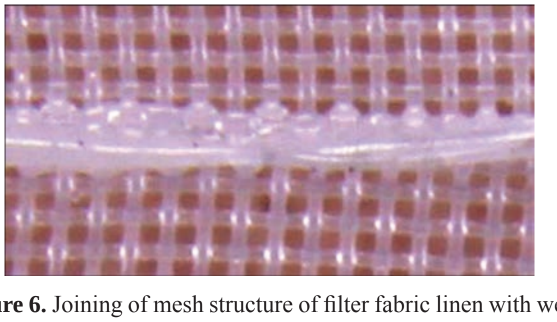

Figure 6. Joining of mesh structure of filter fabric linen with weld material

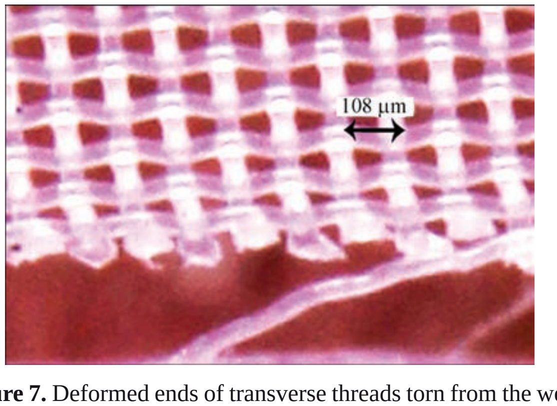

Figure 7. Deformed ends of transverse threads torn from the weld of mesh fabric

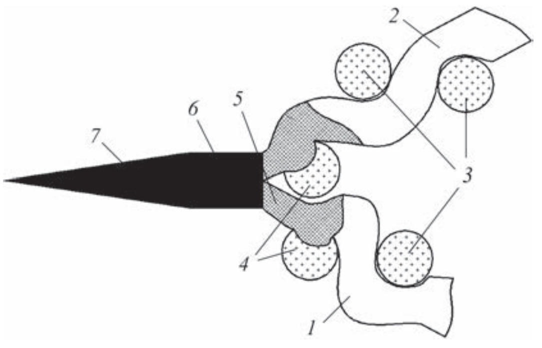

Figure 8. Scheme of formation of cut-out T-shaped weld of mesh filter fabric: *1*, *2* — lower and upper cross threads; *3* — longitudinal undeformed threads; *4* — longitudinal partially melted threads; *5* — shape changes at the places of joining transverse threads; *6* — solid hardened weld; *7* — «tail» of a solidified melt formed during welds disjoining

ven material, the corresponding parts of them melt and participate in the formation of a pool of a homogeneous melt. Through the zone of transition from the polymer melt to the unconverted fibrous polymeric material of the thread, the line of joining of the fabric to be welded is formed. In the scheme, Figure 8 it is shown that the thickness of the threads in these places is significantly reduced as a result of their flattening, as far as the wire of the heating tool with a diameter of 800 μm acts as a punch on the thread with an average diameter of 40 μm.

After completion of heating and removal of the heating tool, the array of a solid polymer melt hardens and forms a hard weld along the entire welding line. Since in this case welding with cutting takes place, two longitudinal welds are simultaneously formed on both sides of the heater string. The volume of a molten material of threads is small, so the transverse dimensions of the hard weld amount to fractions of a millimeter. On the other hand, at the moment of disjoining the parts of the fabric cut by heating, strands from the melt are formed, which after hardening in some places of the weld «tails» in the form of fibers of different shapes and lengths form.

Thus, joining the mesh fabric with the rigid weld occurs through the deformed flattened sections of the transverse threads, the strength of which is certainly reduced as compared to the basic strength of the thread. Each thread of the fabric has a complex inner structure and is woven from several tens of primary staple or continuous polyester fibers. In a welded joint, in the flattened areas these fibers are partially torn, change the angle of inclination and mutual orientation. It is almost impossible to preserve an undamaged fibrous structure of the thread during welded joint formation.

Mechanical tests of welds of a filter polyester fabric produced by heat-pulse welding showed that the maximum level of their mechanical tensile strength does not exceed 60–70 % of the level of the base material. Taken into account the high primary strength of woven polyester material, such strength of welds is quite sufficient for reliable service of filter bags made of it. After turning out, welded filter bags are completely ready for use. Taking into account the small level of mechanical loads on the fabric and welds of the bag during its service as a part of a laboratory installation, in order to test the quality of finished products, it is sufficient to visually inspect the welds to detect lacks of penetrations or other obvious defects.

Conclusions

The studies showed that the most effective method of joining a mesh filter polyester fabric is heat-pulse welding. The technology of manufacturing filter bags from polyester mesh fabric using a modified scheme of heat-pulse welding with welt seams with a full penetration and simultaneous cutting of welded material was developed. A welding installation was created, the studies of morphology and strength characteristics of welded joints produced by means of a modified method of heat-pulse welding were carried out. It was determined that produced welded joints meet the necessary criteria for the intended use of products made of corresponding ultra-thin woven fabrics.

1. Arzhakov, M.S., Zhirnov, A.E., Efimova, A.A. et al. (2012) *Macromolecular compounds*. Moscow, MGU [in Russian].
2. Buketov, A., Brailo, M., Yakushchenko, S., Sapronova, A. (2018) Development of epoxy-polyester composite with improved thermophysical properties for restoration of details of sea and river transport. *Advances in Materials Sci. and Engineering*, 1–6. Doi: https://doi.org/10.1155/2018/6378782.
3. Buketov, A., Brailo, M., Yakushchenko, S. et al. (2019) Investigation of tribological properties of two-component bidisperse epoxy-polyester composite materials for its use in the friction units of means of sea transport. *Periodica Polytechnica Mechanical Engineering*, 63(**3**), 171–182. Doi: https://doi.org/10.3311/PPme.13161
4. *Polyester Manufacturing*. http://www.teonline.com/knowledge-centre/polyester-manufacturing.html
5. Savostitskiy, N.A., Amirova, E.K. (2012) *Materials science of clothing manufacture*. Moscow, Akademiya [in Russian].
6. DSTU 2004. ISO 5498:1981. *International Standards Office. Agricultural food products. Determination of crude fibre content. General method*.
7. Jevsnik, S., Vasiliadis, S., Bahadir, S. K. et al. (2016) Applying heat for joining textile materials. In: *Joining Technologies. Intech Open*. Doi: https://doi.org/0.5772/64309.
8. Midha, V.K., Dakuri, A. (2017) Spun bonding technology and fabric properties: A review *J. Textile Eng. Fashion Techno.*, 1(**4**), 126–133. Doi: https://doi.org/ 10.15406/jteft.2017.01.00023.
9. *Filter polyester cloth of trade mark Saatifil*. http://www.saati.com/images/filtration/tds-saatifil-polyester.pdf

Received 21.02.2021

https://doi.org/10.37434/tpwj2021.07.05

SKIN-EFFECT IN SOFT BIOLOGICAL TISSUE AND FEATURES OF TISSUE HEATING DURING AUTOMATIC BIPOLAR WELDING

V.G. Solovyov, Yu.M. Lankin and **I.Yu. Romanova**
E.O. Paton Electric Welding Institute of the NAS of Ukraine
11 Kazymyr Malevych Str., 03150, Kyiv, Ukraine. E-mail: office@paton.kiev.ua

The skin-effect that occurs in the electric circuit at high-frequency electrosurgery, including electric welding of soft biological tissues (SBT) with electrodes for bipolar welding, is of interest to researchers as a possible source of considerably uneven heating of SBT in automatic welding. Mathematical study of electrical and thermal processes in automatic bipolar welding was performed, taking into account and ignoring the impact of skin-effect at the frequency of 300 kHz. It was determined that in biological tissue the skin-effect causes uneven heating to a smaller degree. The main reasons that influence the unevenness of heating are the presence of sharp ridges on the surface of electrodes that contact the tissue, degree of SBT compression by the electrode clamps, length of SBT compressed between the electrodes, and also duration of the process of SBT heating. 13 Ref., 6 Figures.

Keywords: *skin-effect, bipolar electrodes, electric welding of soft tissues, biological tissue, anisotropy of specific conductivity*

Electrosurgery with application of high frequency currents (HFC) of more than 200 kHz [1] became widely applied in medicine. Passage of HFC through the electric circuit of the conductors, which are the electrodes of electrosurgical instruments, and a section of soft biological tissues (SBT) being welded, generates a high-frequency electromagnetic field that leads to current density concentration near the conductor surface. So-called surface effect (skin-effect) arises [2]. Nonuniform distribution of current density results in nonuniform distribution of Joulean heat in the conductor cross-sectional plane. One of the quality requirements to electric welding of soft tissues is even heating of SBT section being welded. In this connection, a number of researchers in their work paid attention to the evenness of SBT heating during performance of electrosurgical operations, allowing for the skin-effect. Works [3, 4] analyze the influence of skin-effect arising at the frequency of 440 kHz in a thin cylindrical monopolar electrode at welding of the retina, which has detached, to the choroid. Coagulation rings as traces of current passage, are clearly visible under the microscope. The question of modeling the skin-effect in the electrode is considered in detail, but no analysis of the electric and thermal processes in SBT at appearance of coagulation rings on the choroid is given. In works [5–8] the main attention is paid to elimination of the nonuniformity of current density distribution in the electrodes in the presence of skin-effect, but without analyzing how this nonuniformity affects the distribution of Joulean heat in SBT.

The objective of the work is to show the results of mathematical analysis of running of the electric and thermal processes in SBT (pig heart muscle) at automatic bipolar welding with different degrees of tissue compression between the electrodes, taking into account the skin-effect at 300 kHz frequency, as well as in the assumption of absence of the skin-effect.

Model, used to conduct the mathematical experiment of skin-effect impact on SBT, was constructed using COMSOL Multiphysics 5.3a software package. The model includes «Electric Currents» and «Heat Transfer in Solids» («physics») modules with «Multiphysics/Electromagnetic Heating» solver which allows combining these different physics to solve the model tasks. Pig heart muscle and copper jaw plates (electrodes) were taken as materials used in the model. The range of the set electrode pressure was 15–1100 kPa. Electrode cross-section was 3×10 mm. Dimensions of the heart muscle fragment were equal to: initial thickness of uncompressed tissue *mh* = 6.9 mm, width — 35 mm and depth — 25 mm. The compression coefficient is taken into account by the following formula

$K_{\text{com}} = \left(1 - \dfrac{hs}{mh}\right) \cdot 100\ \%$, where *hs* is the thickness of SBT between the electrodes.

V.G. Solovyov — https://orcid.org/0000-0002-1454-7520, Yu.M. Lankin — https://orcid.org/0000-0001-6306-8086,
I.Yu. Romanova — https://orcid.org/0000-0001-7154-1830

Proceeding from the postulates of the theory of similarity [9], a model was created in COMSOL Multiphysics package that takes into account the similarity of its geometrical parameters to those of the physical model. Modeling allowed determination of the anisotropy of specific electric conductivity in the zone of SBT local compression (Figure 1) [10].

The main condition for modeling was to ensure the best correlation between the geometrical part of the model and geometrical parameters of the physical experiment. Here, it was necessary to use the physical properties of pig SBT that correspond to the heat muscle, taking into account the anisotropy of its specific conductivity at compression.

Mathematical experiment was conducted at the frequency of alternating harmonic current $f = 300$ kHz.

For a field that oscillates with frequency f, we have:

$$\Delta \sim 50\sqrt[3]{(\sigma\mu f)^{-1}} \qquad (1)$$

where Δ is the skin-layer thickness, m; σ is the specific conductivity, S/m; μ is the relative magnetic permeability, rel. un.

If the thickness of the skin-layer is great, compared to body dimensions ($\Delta >> lh$), the distribution of the magnetic field at each moment of time will be the same as in the stationary case at the specified value of the field outside of the body. Here, the vortex electric field and the resistive losses related to it, can be neglected [11].

Taking into account the anisotropy of specific conductivity in the zone of SBT local compression (Figure 1), we can calculate the dependence of Δ on K_{com}. Calculations show that the smallest thickness of the skin-layer for the conditions of our experiment is equal to 1.7 m (Figure 2). This is much more than the dimensions of that electromagnetic field, acting around the electrodes with 3×10 mm cross-section. As is known, SBT electric welding differs from electrocoagulation by mandatory application of a considerable force of electrode compression [12]. Electrode pressure leads to (possible) destruction of the cell membranes, to transfer of electrically conductive tissue water from the electrode center to the periphery in the direction of pressure lowering, to increase of vapour formation temperature and maximum temperature of the tissue. In this connection, at maximum degree of compression of the pig heart muscle K_{com} = = 78 %, the skin-layer thickness (Figure 2) is 2.5 m.

Taking into account the above-said, it can be stated with a high degree of probability that the high-frequency current passing through SBT should cause practically no changes in current density distribution in SBT under the conditions of electrosurgical operations on soft biological tissues.

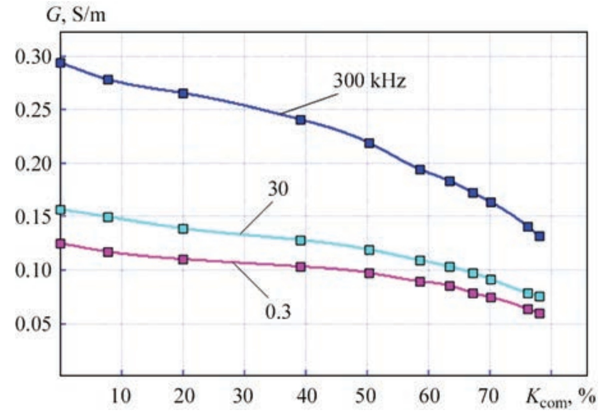

Figure 1. Dependence of specific electric conductivity of pig heart muscle G on the degree of compression K_{com} for frequencies of 0.3, 30 and 300 kHz

Hence the question: what is happening with distribution of current density on the electrode surface at their collision with SBT. As SBT is an element of the circuit where HFC flows, there should be no nonuniformity of current associated with the skin-effect, on the boundary of electrode contact with SBT. However, a reverse situation was observed with coagulation rings on the retina in work [3].

In our model the electrodes are represented by copper jaw plates. HFC flows from the voltage source through the copper plate of 3×10×1.5 mm size, then through a section of SBT, compressed by the electrodes, and then through the second copper plate. The electric circuit is closed to the voltage source.

Even for a round conductor calculation of the skin-effect involves considerable difficulties. In order to perform the calculation, many assumptions are used of the conductor straightness, infinity of its length, etc. For conductors of a rectangular cross-section, in work [13] calculation is based on the assumption that the conductor cross-section consists of sets of round conductors, the diameter of which is equal to doubled thickness of the skin-layer, and, accordingly, on the assumption of the conductor straightness and infinity of its length.

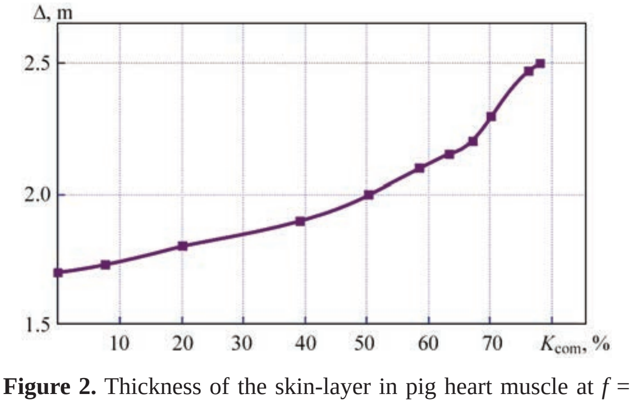

Figure 2. Thickness of the skin-layer in pig heart muscle at f = = 300 kHz, depending on the degree of compression

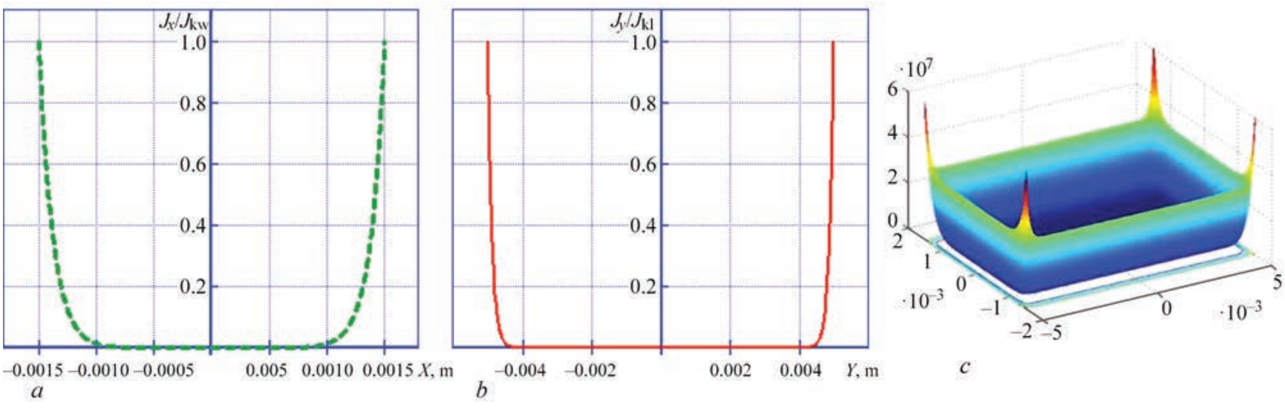

Figure 3. Graphs of distribution of relative current density along the width (*a*) and length (*b*) of the jaw copper plate and distribution of 3D specific conductivity in 3D image (*c*)

For our model we take the following assumptions, in order to simplify calculation of the skin-effect impact:

● skin-effect is present only in the jaw copper plates;

● as the skin-effect is manifested in the current density concentration on the conductor surface, we perform simulation of the skin-effect through assigned nonlinearity of specific conductivity along the length and width of the copper plate;

● dependence of reduction of the current density on frequency in copper when moving away from the surface is readily approximated by hyperbolic cosinus;

● skin-effect is manifested both along the width, and along the length of the copper plate, here the current density is averaged.

We will denote half-width of the copper plate as a_w, its half-length as b_l. Then, a_w = 1.5 mm, b_l = 5 mm. X coordinate of the plate with be in the range of $\{-a_w \ldots a_w\}$. Y coordinate of the plate will be in the range of $\{-b_l \ldots b_l\}$. Current density J_x along X coordinate is calculated by the following formula:

$$J_x = \mathrm{ch}(kf^{0.5}X), \quad (2)$$

similarly, for

$$J_y = \mathrm{ch}(kf^{0.5}Y). \quad (3)$$

On the left and right surfaces of the copper plate, limiting its width, current density will be $J_{kw} = \mathrm{ch}(kf^{0.5}a_w)$. Accordingly, on the opposite surfaces, limiting the plate length, current density will be $J_{kl} = \mathrm{ch}(kf^{0.5}a_a)$. Value of coefficient k is determined by inverse transformation of hyperbolic cosines in formulas (2) and (3) and substitution of the value of skin-layer thickness for copper at the frequency of 300 kHz, obtained using (1). As for copper Δ = = 0.119 mm, then k = 15.36.

In connection with the fact that current density J is proportional to specific conductivity σ of an elementary site of normal current vector, we assume that:

$$\sigma(X,Y) = 6E^7\left(\frac{J_x(X)}{J_{kw}} + \frac{J_y(Y)}{J_{kl}}\right)0.5.$$

Substituting σ(X, Y) in the calculation part of the model for the value of specific conductivity of copper, which is unchanged in each elementary volume of the copper plate (σ = 6E^7, S/m) for direct current, we obtain the current density distribution in the copper jaw plates, that corresponds to the distribution at the skin-effect for 300 kHz frequency. Figure 3 presents the graphs of distribution of the relative current density along the width and length of the jaw copper plates, as well as a 3D image of σ (X, Y).

To gain a more definite understanding of current density distribution at skin-effect inside the copper plate volume, including within the SBT, we will calculate the current distribution along lines A and B (Figure 4, *a*, *b*). Line A lies in the plane, which is the boundary between the copper plate and SBT (SBT not shown in the figure for simplification purposes), and it passes in the middle of the plate along its width. Line B passes between the center of the surface of the plate left side and center of the surface of the copper plate right side. In Figure 4, *a* we can see that the current density along line B decreases from the left surface of the copper plate from 28000 A/m^2 practically to zero, and then rises towards the right surface of the plate up to 28000 A/m^2. Distribution of current density along line A is repeated with the same regularity, but it has much smaller values at the ends (approximately 2000 A/m^2), while middle value of current density is higher than that for line B.

In order to refine the results, we will calculate the current density distribution along the secant segment connecting the centers of line B and line A (Figure 4, *c*), as well as the secant segment connecting the left ends of these lines (Figure 4, *d*).

It is obvious that when getting closer to SBT, the current density abruptly changes its values, the first

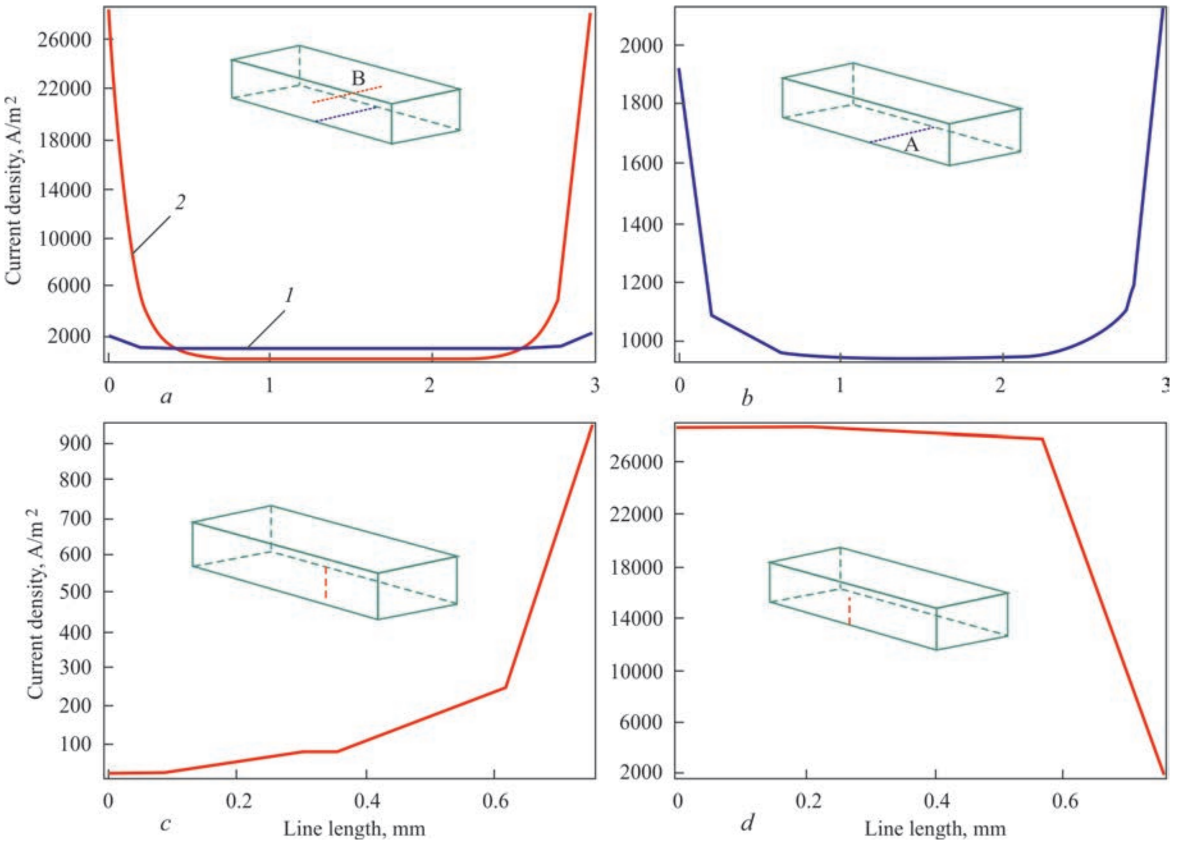

Figure 4. Distribution of current density at skin-effect within the copper plate along lines A and B (*a*) (*1* — distribution of current density along line A; *2* — along line B) and A (*b*). Distribution of current density at skin-effect within the copper plate along a vertical secant connecting the centers of lines B and A (*c*) and secant connecting the left ends of lines A and B (*d*)

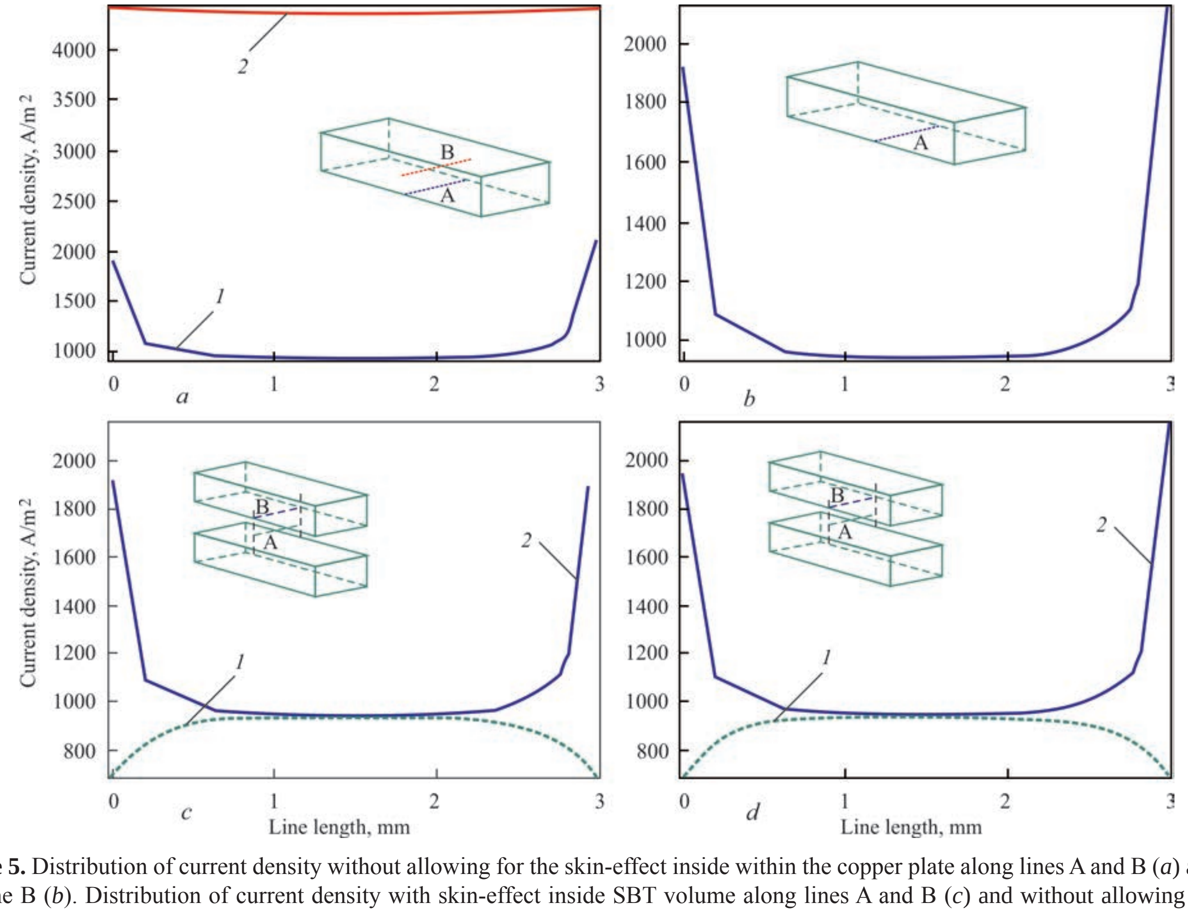

Figure 5. Distribution of current density without allowing for the skin-effect inside within the copper plate along lines A and B (*a*) and just line B (*b*). Distribution of current density with skin-effect inside SBT volume along lines A and B (*c*) and without allowing for skin-effect (*d*) (*1* — distribution of current density along line A; *2* — along line B)

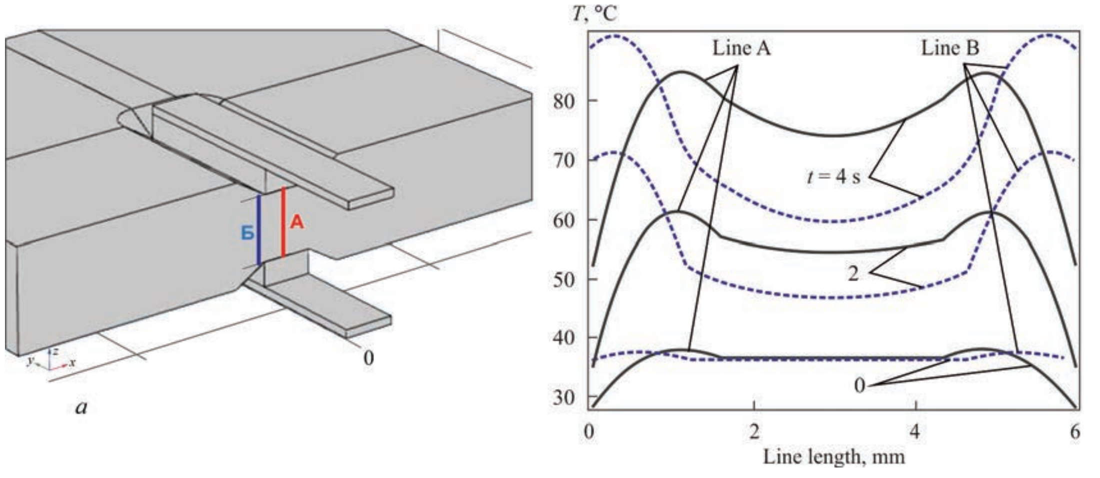

Figure 6. Vertical lines A and B on SBT surface (*a*). Temperature distribution in SBT along axis *Z* along vertical lines A and B at moments of time 0, 2 and 4 s (*b*)

(Figure 4, c) towards its increase, and the second (Figure 4, *d*) towards its decrease. This is indicative of the fact that the electric properties of SBT have a dominating impact on current density distribution in the copper plate near SBT.

Then we will calculate current distributions along the same lines, as in the previous calculations, but we will eliminate the simulation of the skin-effect (Figure 5, *a*, *b*). Distribution of current density along line B is practically uniform, and is equal to approximately 5000 A/m^2, while distribution of current density along line A is the same as current distribution, calculated at skin-effect (Figure 4, *b* and Figure 5, *b*).

Thus, we obtained one more confirmation that the skin-effect is practically absent in biological tissue at bipolar welding.

Further calculations of current density distributions inside the biological tissue along lines A and B with «included» skin-effect (Figure 5, *c*) and along the same lines without the skin-effect (Figure 5, *d*) showed complete identity of the results.

Note the fact that the current density in the middle of line A and in the middle of line B coincides (Figure 5, *c*, *d*). Therefore, SBT middle part, compressed between the electrodes, has the same specific electric conductivity along the vertical. At a distance from the middle to the left and right from line A the specific conductivity decreases, because of approaching the SBT sections with lower compression. With greater distance from the middle to the left and right along line B the current density grows, because of approaching the copper plate ridges, on which an increase of electric field density is observed, because of an abrupt increase of the conductor curvature. Such a nonuniform distribution of current density on electrode-SBT boundary results in appearance of a nonuniform distribution of the thermal field on the tissue surface.

Temperature distribution was calculated along vertical line A in SBT (Figure 6, *a*) between the electrode middles and along line B, which has equal length with line A and passes vertically to the left of the lower corner of the copper plate by 0.05 mm. Calculation was performed for three moments of heating time: 0, 2 and 4 s. The graph (Figure 6, *b*) shows that after 4 s of heating the temperature at the ends of line B has reached the critical value of ~90 °C, and the temperature inside SBT compressed section on line A was ~70 °C. Such a unevenness of SBT heating can lead at the stage of dehydratation in some sections of the tissue to unplanned coagulation processes, and as the polymerization stage tissue necrosis can occur in some sections.

Most probably, the coagulation rings on the retina, described in work [3], formed because of higher current density on the electrode ridges. It is envisaged that the rounding-off of the ridges on the electrode surface, located on the boundary with SBT, will allow partially eliminating the unevenness of heating distribution in SBT at mono- and bipolar welding.

Conclusions

1. The conclusion that the skin-effect, arising at HFC passage through the jaw copper plates, does not influence the processes of current flowing and SBT heating, is important for solving the tasks of automation of bipolar welding of SBT.

2. Nonuniformity of current density in SBT and running of the heating processes are affected by presence of sharp ridges on the surface of electrodes, contacting the tissue, coefficient of SBT compression by electrode clamps, length of SBT compressed between the electrodes, as well as time of running of SBT heating process.

3. The model developed during the mathematical experiments, using COMSOL multiphysics, will further allow studying the procedure of selection of the required ratios of geometrical parameters of the electrodes, selection of the laws of automatic change

of supply voltage (current) in time, in order to reach an optimum heating process at automated welding of soft biological tissues to improve the quality of the produced welded joints.

1. DSTU EN 60601-2-2:2019 (EN 60601-2-2:2009, IDT; IEC 60601-2-2:2009, IDT) *Medical electrical products.* Pt 2-2. *Additional safety requirements and basic performance of high frequency surgical equipment and high frequency surgical accessories* [in Russian].
2. Polivanov, K.M. (2015) *Theoretical principles of electrical engineering. Pt. 3: Theory of electromagnetic field.* Moscow, Energiya [in Russian].
3. Sydorets, V.M., Dubko, A.G. (2015) Distribution of current in electrodes of electrosurgical instruments in welding of biological tissues. *Eastern-European J. of Enterprise Technologies*, **3**, 24–28 [in Ukrainian]. DOI: https://doi.org/10.15587/1729-4061.2015.43372.
4. Sydorets, V., Dubko, A., Bondarenko, O., Kosenko, R. (2016) Influence of skin-effect on current flow through electrodes of electro-surgical instruments and biological tissue. In: *Proc. of 15th Biennial Conf. on Electronics and Embedded Systems (BEC-2016, Tallinn, Estonia)*, 211–214.
5. Sydorets, V.M., Dubko, A.G. (2015) Peculiarities of analysis of high-frequency current distribution in axisymmetric electrodes for electrosurgical instruments. *Elektrotekhnika ta Electroenergetyka*, **2**, 42–47 [in Russian].
6. Sydorets, V., Lebedev, A., Dubko, A. (2015) Mathematical modeling of the current density distribution in a high-frequency electrosurgery. In: *Proc. of 16th Int. Conf. on Computational Problems of Electrical Engineering (CPEE, Lviv, Ukraine)*, 215–217. DOI: https://doi.org/10.1109/CPEE.2015.7333379.
7. Dubko, A., Sydorets, V., Bondarenko, O. (2018) Simulation of the temperature distribution with high-frequency electrosurgical heating. In: *Proc. of 38th Int. Conf. on Electronics and Nanotechnology (ELNANO – 2018, Kyiv, Ukraine)*, 394–397.
8. Dubko, A.G., Chvertko, N.A., Lebedev, O.V. et al. (2020) Mathematical models of density distribution of high-frequency current in electrodes with different shapes of transverse cross-section. B*iomedychna Inzheneriya i Tekhnologiya*, **3**, 92–98 [in Ukrainian].
9. Gukhman, A.A. (1973) *Introduction to similarity theory.* 2nd Ed. Moscow, Vysshaya Shkola [in Russian].
10. Lankin, Yu.M., Solovyov, V.G., Romanova, I.Yu. (2021) Study of change in specific electrical conductivity ob biological tissues as a result of local compression by electrodes in bipolar welding. *The Paton Welding J.*, **1**, 35–39. DOI: https://doi.org/10.37434/as2021.01.07
11. Pegel, I.V. (2009) *Electrodynamics of superhigh frequency:* Manual. TPU [in Russian].
12. Shved, O.E. (2008) *Substantiation of new surgical method of hemostasis (experimental-clinical study):* Syn. of Thesis for Cand. of Med. Sci. Degree, Kyiv [in Ukrainian].
13. Bulgakov, O., Petrov, S., Lupandin, V. (2009) Allowing for skin-effect in problems of self-induction and mutual induction induced by current flow in conductor with rectangular cross-section. *Komponenty i Tekhnologii*, **4**, 122–125 [in Russian].

Received 23.03.2021

https://doi.org/10.37434/tpwj2021.07.06

EVALUATION OF DAMAGE OF ALL-WELDED LONGITUDINAL MAIN BEAMS OF THE E.O. PATON BRIDGE ACROSS THE DNIPRO RIVER

V.D. Poznyakov, V.P. Dyadin, Ye.O. Davydov and **R.I. Dmytrienko**
E.O. Paton Electric Welding Institute of the NAS of Ukraine
11 Kazymyr Malevych Str., 03150, Kyiv, Ukraine. E-mail: office@paton.kiev.ua

The problem of general evaluation of technical condition of main longitudinal beams of the E.O. Paton Bridge was considered based on the results of selective non-destructive testing of truss elements. It is shown that the main cause of damage to the elements of the main beams is corrosion of the nodal welded joints in the places of debris accumulation. High quality of welded butt joints made by automatic and semi-automatic submerged arc welding was noted. 10 Ref., 18 Figures.

Keywords: E.O. Paton Bridge, main beams, welded joint, corrosion, non-destructive testing, technical diagnostics, automatic and semi-automatic welding, damage to welded joints

The E.O. Paton Bridge across the Dnipro River in Kyiv has been in operation since 1953. It is the world's first all-welded road bridge which entered the annals of the world bridge construction. Prior to the commissioning of this structure, all bridges had riveted joints of elements. Single attempts in building welded bridges had so far failed. That fact was first of all associated with a sharp drop in the load-carrying capacity of welded joints during manufacture of large-sized metal structures. The main cause for such a drop was a simple replacement of riveted joints on welded ones without taking into account the stressed state of welded elements and imperfection of welding technologies developed at the time, which led to crack formation both during manufacture (shop and site welding), as well as during operation of welded structures.

Brittle fractures of welded structures in the 1940s began to bear a mass character, the majority of which had a number of features:

● fracture nuclei were usually located at the places of welded joints;

● fracturing occurred at very low operating loads and relatively high temperatures;

● a number of partial fractures of welded structures significantly increased.

Thus, from the 2500 Liberty ships built during World War II, 145 broke in half and 700 were severely damaged. Many bridges and other structures followed the same pattern [1, 2].

Such kind of fractures very strongly stimulated the development of investigations in the field of welded joints and largely determined their direction. A significant contribution to the development of investigations on the load-carrying capacity of welded joints was made by the Laboratory of Electric Welding, which was a part of the All-Ukrainian Academy of Sciences in Kyiv, which later in 1934 was transformed into the Electric Welding Institute of the AS of the UkrSSR.

The experience gained at the Electric Welding Institute in the manufacture of metal structures allowed using the technologies of mechanized submerged arc welding, which were advanced at that time and proved themselves well during the Second World War at enterprises that manufactured hulls of armored vehicles. At that time, E.O. Paton changed the concept of the bridge construction and proposed to make it all-welded applying automatic welding. This approach caused a necessity in the development of new designing solutions for span structures, steel for their manufacture and automatic welding equipment.

As far as welding technologies were still imperfect at that time and could not provide a full evaluation of properties of welded joints, taking into account thermodynamic cycle of welding and residual stresses, the technologies of automatic welding proposed by E.O. Paton significantly improved the quality and strength of welded joints. Namely these welding technologies were taken as a basis and used in the manufacture of metal structures of the E.O. Paton Bridge in the shop conditions, as well as during their assembly on the construction site [3–6]. Among the significant advantages proposed by E.O. Paton over the ap-

V.D. Poznyakov — https://orcid.org/0000-0001-8581-3526, V.P. Dyadin — https://orcid.org/0000-0002-2061-8436,
Ye.O. Davydov — https://orcid.org/0000-0003-3470-2329, R.I. Dmytrienko — https://orcid.org/0000-0001-8842-5051

Figure 1. Welding of longitudinal stiffeners and girth welds of the truss [3]

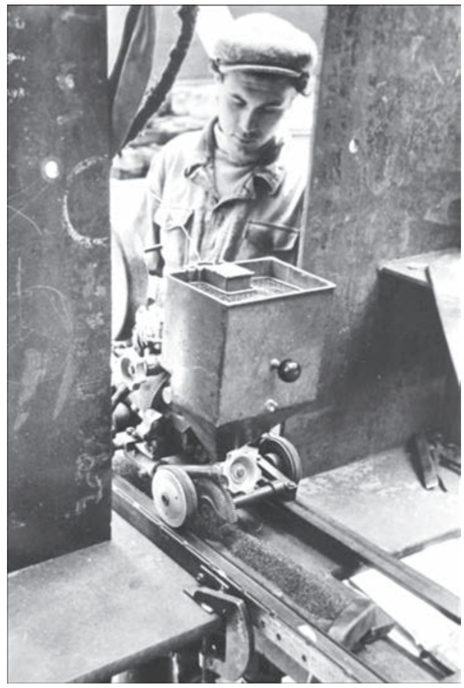

Figure 2. Example of applying automatic submerged arc welding of the lower girth while joining trusses of the main beams [4]

proaches to the construction of steel bridges existing at that time, the following should be noted:

- maximum use of automatic and semi-automatic submerged arc welding at the plant that manufactured structures and at the erection site (Figures 1, 2);
- assembly of large-block elements at the plant that manufactured structures (Figure 1);
- assembly of erection joints to one-type butts of continuous trusses of double-T cross-section (Figure 3), which significantly simplified the assembly of trusses and reduced the time of welding works by using automatic and semi-automatic submerged arc welding;
- development of a special design of the erection joint of trusses with an insert in a vertical wall and an upper flange and a sequence of their joints by means of automatic submerged welding of girths with extension of a weld on additional laths (Figures 2, 3).
- maximum reduction in the use of manual arc welding with coated electrodes;
- development of low-carbon M16C steel, low-sensitive to thermodeformed welding cycle;
- development of new electrode wires and fluxes;
- development of new equipment for automatic and semi-automatic submerged arc welding in a wide range of technological modes of its use in industry.

The complex of these solutions provided the necessary reliability and quality of nodal welded joints of bridge structures (more detailed information can be found in [6]). That is why in 1995 the bridge was recognized by the American Welding Association as an outstanding welded structure of the twentieth century.

The total length of the bridge is 1542.2 m, it consists of 24 spans. The construction of the bridge began from the left bank of the Dnipro River.

The right-bank part of the bridge consists of ten spans, which are overlapped by two all-welded five-span continuous structures — (5×58) + (5×58) m (further indicated as 1–5S and 2–5S).

The middle part of the bridge over the navigable region of the river has six spans, which are overlapped by continuous all-welded structures — 58 + 4×87 + 58 (m) (further indicated as 6S).

The left-bank part of the bridge has 8 spans of 58 m each and is overlapped by two four-span continuous welded structures — (4×58) + (4×58) m (further indicated as 1–4S and 2–4S).

In the cross-section, each structure has four main longitudinal beams of double-T section, consisting of a vertical wall with 3600 mm height and 14 mm thickness and girths of different thickness, varying from 30

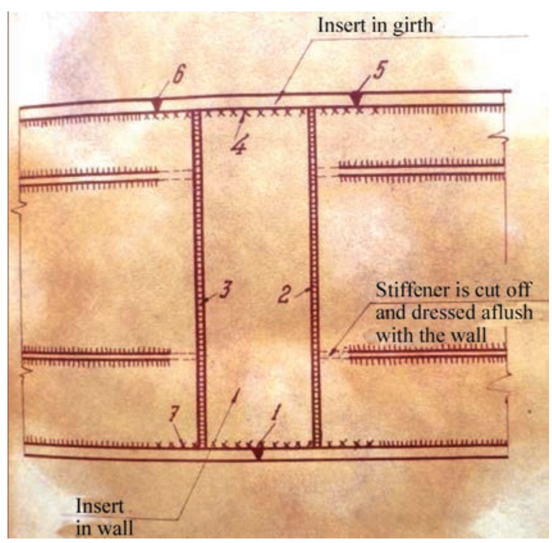

Figure 3. Order of erection assembly and welding of typical bridge trusses [4]

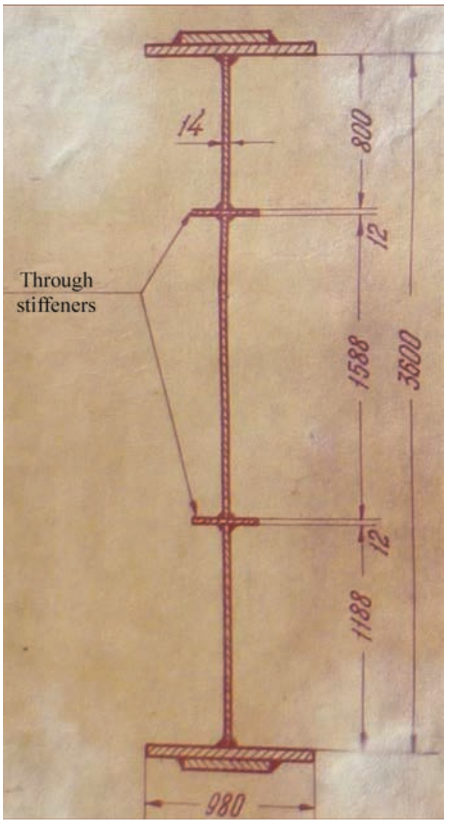

Figure 4. Cross-section of the truss of the main longitudinal beams of four- and five-span structures of the bridge [4]

to 80 mm, with a width of up to 1000 mm (Figure 4). The stability of the beam wall is additionally provided by vertical stiffeners mounted with a step of 7.25 m.

In six-span structures, the height of the wall above the intermediate supports is increased to 6200 mm due to built on haunches.

The main longitudinal beams are composed of trusses, which are butt-welded using automatic submerged arc welding during erection of metal structures. A number of trusses in each of the four-span main longitudinal beams is 9 pcs, in the five-span main beams there are 11 pcs, and in the six-span main beams there are 21 pcs. The trusses are made of low-carbon steel of M16C grade.

The E.O. Paton Bridge across the Dnipro River in Kyiv was designed based on the conditions that the designed traffic intensity should be 10 thou cars per day. During a long-term operation of the bridge, the load on its load-carrying elements gradually increased, which is associated both with an increase in the traffic intensity per day (currently it has increased by almost 10 times — during «peak» hours — up to 85 thou per day), as well as with an increase in car weight [7]. As a result of laying pipes of the heat pipeline and increasing the thickness of the asphalt concrete pavement, the constant loads on the bridge also increased. Taking that into account, in 1994–1998 the transverse beams of the bridge, which are located near the expansion joints, were reinforced, and additional stiffeners were mounted on some regions of vertical walls of the main beam trusses [7].

Until 2019, the main longitudinal beams of the bridge were inspected only visually without the use of instrumental and physical methods of testing, which did not allow obtaining more detailed information on the actual technical condition of metal structures [7, 8]. Thus, according to the results of inspection of the bridge, performed at the end of 2018 by the specialists of LLC «V.M. Shimanovsky Ukrainian Institute of Steel Construction», it was pointed out that on the walls of the main beams of the structure in the locations of expansion welds, the formation of a layer of corrosion products was observed. Considering and analyzing the results of investigations, V.M. Shimanovsky Ukrainian Institute of Steel Construction came to the conclusion that the E.O. Paton Bridge is in an emergrency situation and urgently needs major repairs with a partial replacement of its structural elements. This issue was repeatedly discussed at the meetings in the Kyiv City State Administration and «Kyivavtodor», on the results of which a decision was made on the reconstruction of the bridge and a need for a more detailed inspection of its structural elements. In 2019, the works on evaluation of general technical condition of the bridge were entrusted to LLC «V.M. Shimanovsky Ukrainian Institute of Steel Construction» with the involvement of specialists of the E.O. Paton Electric Welding Institute of the NAS of Ukraine in terms of inspection of the main longitudinal beams of the bridge.

Inspection of the technical condition of the main beams of the bridge structures was performed in 2020. A part of the results of the investigations conducted by the experts of the PWI is given in [9]. The investigations were conducted in the following areas:

- selective ultrasonic testing of butt shop and erection welded joints of beams and base metal of beam elements for the presence of delamination;
- thickness measurement of the main elements of the main beams at the access points;
- selective magnetic control of fillet and butt welded joints.

The choice of such testing methods was determined based on the results of the previous inspection of the main longitudinal beams of the bridge located between the 2nd and 3rd supports, which was performed by the specialists of the PWI (in July 2019), taking into account data [10]. 100 % visual inspection of welded jonts was also completed. According to the results of the previous inspection, the main areas of investigations were determined, which can be divided into three components:

Figure 5. Example of testing butt vertical welds of the joining insert

● detection of a possible fatigue damage of welded joints after a long-term operation;

● evaluation of integrity of the base metal from which the elements of trusses are made;

● evaluation of the sizes of a corrosion damage of the elements of trusses and welded joints of the main beams.

The main attention during the selective ultrasonic testing of butt welds was paid to the places where defects were detected during the erection and manufacture of truss elements [3, 4, 9], and to the maximum stressed areas. At a total length of erection and shop welded joints of about 110 km, 150 m of welded joints were inspected, 50 % of which amounted to erection welds at the places of joining trusses (Figures 2, 3, 5, 6).

Considering that the ultrasonic method of testing does not provide a reliable control of surface and near-surface layers in a welded joint, the magnetic method of testing was additionally applied. Magnetic control was performed in different places of span structures on 124 sections of welded joints with a total area of 40.0 m^2. Taking into account the more complex conditions of erection, more attention was paid to erection welded joints using the method of magnetic control. All places where non-destructive testing was performed were entered into the operation charts of testing, which were linked to the numbers of trusses from which the longitudinal beam was made and the numbers of supports between which it was located.

Visual inspection of welded joints and analysis of the results of ultrasonic and magnetic control of erection and shop welds of span structures indicate that welded joints of the main beams are in satisfactory condition. Fatigue cracks in welded joints after a long-term operation were not formed. Even those

Figure 6. Example of testing butt weld in the upper girth of the joining insert

defects that were detected already at the stage of construction of the bridge, did not propagate in the process of a long-term operation (Figure 7).

The obtained testing results once again confirm that the proposed designing solutions for a large-block assembly and the principle of maximum use of automatic and semi-automatic submerged arc welding laid at the plant and erection area allowed providing a guaranteed high quality of welded joints. A significant role in achieving these results belongs also to the developed equipment and proposed advanced technologies for welding and assembly of large-block elements (trusses)).

Checking the integrity of the base metal of the main beams by a non-destructive method of testing was associated with the fact that in the manufacture of trusses of the main longitudinal beams in some cases local places with delamination in the metal of horizontal stiffeners were detected. In some cases, when delaminations detected during the manufacture and erection did not reach welded joints, such areas were not repaired [3]. In these places, to evaluate the probable further growth of delamination, 7 m^2 of metal sur-

Figure 7. Example of absence of growth of a defect left during erection (ends of the crack were arrested by drilling method) [4]

Figure 8. Area of debris accumulation and condition of inspection passages on the inner side of the end beam of the five-span structure

face was selectively inspected. The areas of the base metal of different thicknesses were inspected, which were directly adjacent to the welded joints, in which delamination was detected during erection. In none of the tested places the propagation of delamination to other areas was detected.

When designing horizontal stiffeners, their welding-on to the vertical wall of the truss without a full penetration was provided (Figure 4), which significantly reduced the residual stresses over the thickness of the metal and, as a result, considerably lowered the risk of propagating this defect.

In general, the results of carried out investigations showed that in the process of long-term operation, fatigue cracks were not formed in the welded joints of the metal structures of the main beams and these joints are in satisfactory condition.

According to the preliminary conclusions from the obtained results of selective technical diagnostics of the main longitudinal beams [9], the main cause that can significantly reduce the further service life of the bridge is corrosion. During the period of operation, the metal of the main beams has suffered some loss

Figure 9. Area of debris accumulation on the outer side of the end beam of the five-span structure

Figure 10. Area of debris accumulation in the supporting part of the four-span structure

of thickness from corrosion. This was especially observed in the areas of large debris accumulation on the lower horizontal stiffeners, the lower girths of the end beams and at the ends of the supports of the span structures (Figures 8–10).

To specify and determine the most typical damages of the main beam elements and related factors during the inspection of span strucutres with the help of thickness measurements, a number on of which the end beams (No.1, No.4) was significantly higher than on the beams No.2 and No.3. An increased number of measurements was caused by a limited access to the tested elements as a result of an unsatisfactory con-

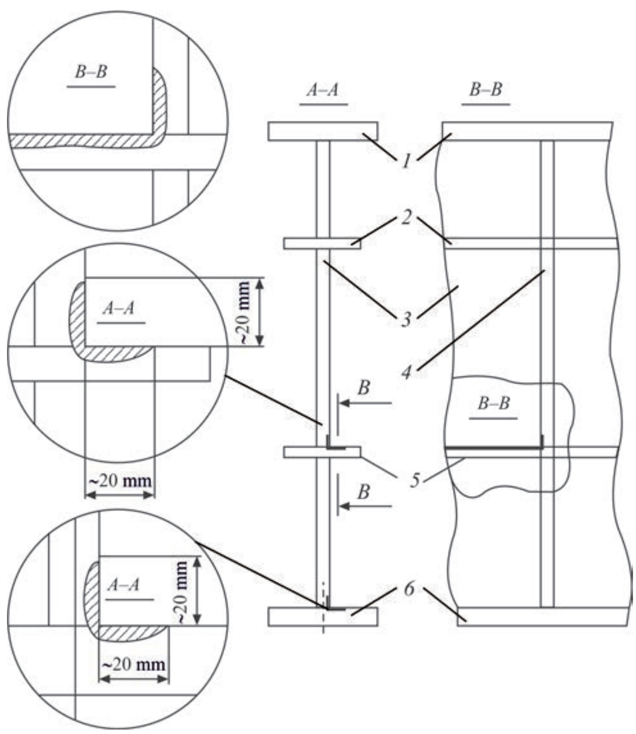

Figure 11. Typical corrosion damages of welded joints of truss elements of the main beams: *1* — upper flange; *2* — upper horizontal stiffener; *3* — wall; *4* — vertical stiffener; *5* — lower horizontal stiffener; *6* — lower flange

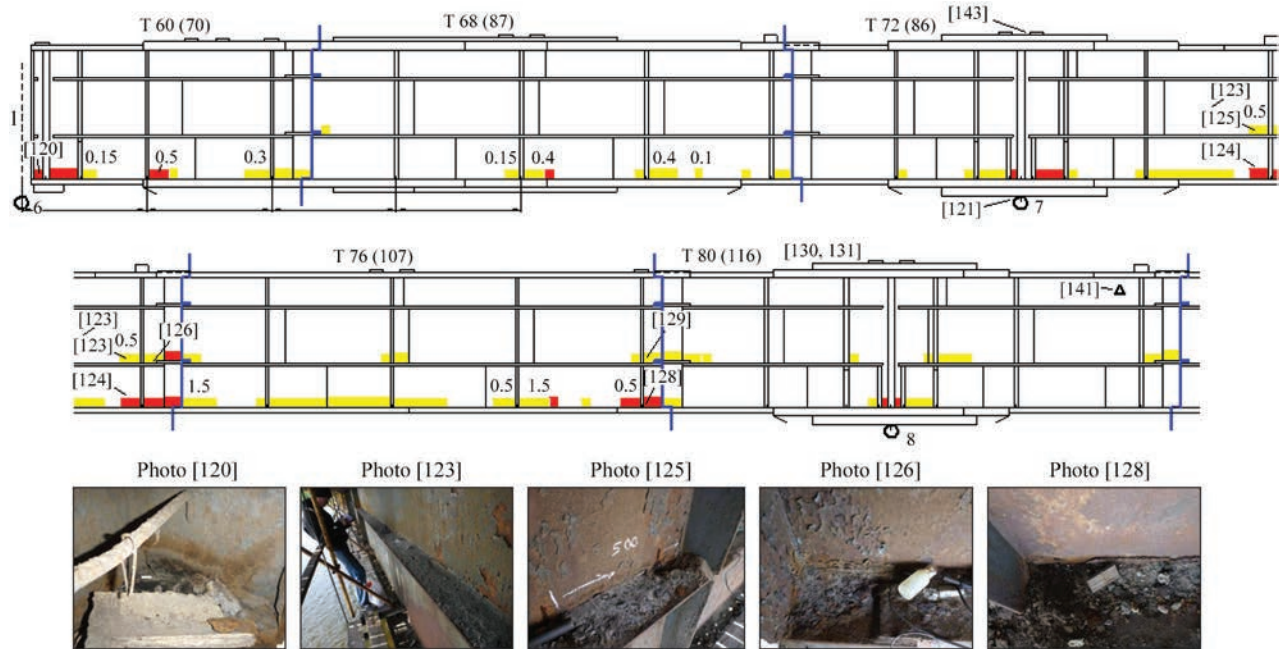

Figure 12. Fragment of tabulated results of testing elements of the beam No.1 of the five-span structure located between the 6-9 support

dition of the inspection passages and a large debris accumulation on the end beams of the structures.

In selective testing of thickness of the truss elements in places of debris accumulation, 12640 measurements were carried out. In total, 16876 measurements of thickness were carried out during a partial inspection of the main longitudinal beams of the span structures, which were entered in the operation charts of the testing (168 truss charts) with a record of the section, where testing was carried out and on the generalized schemes of span structures. The most typical places of corrosion damages of welded assemblies of the main beams of the bridge are presented in Figure 11.

As an example, Figures 12, 13 present the sections with detected corrosion damages and a delamination of the main beams of span structures.

On the given fragments, the following symbols are used (Figures 12, 13): T is a truss; the areas where the

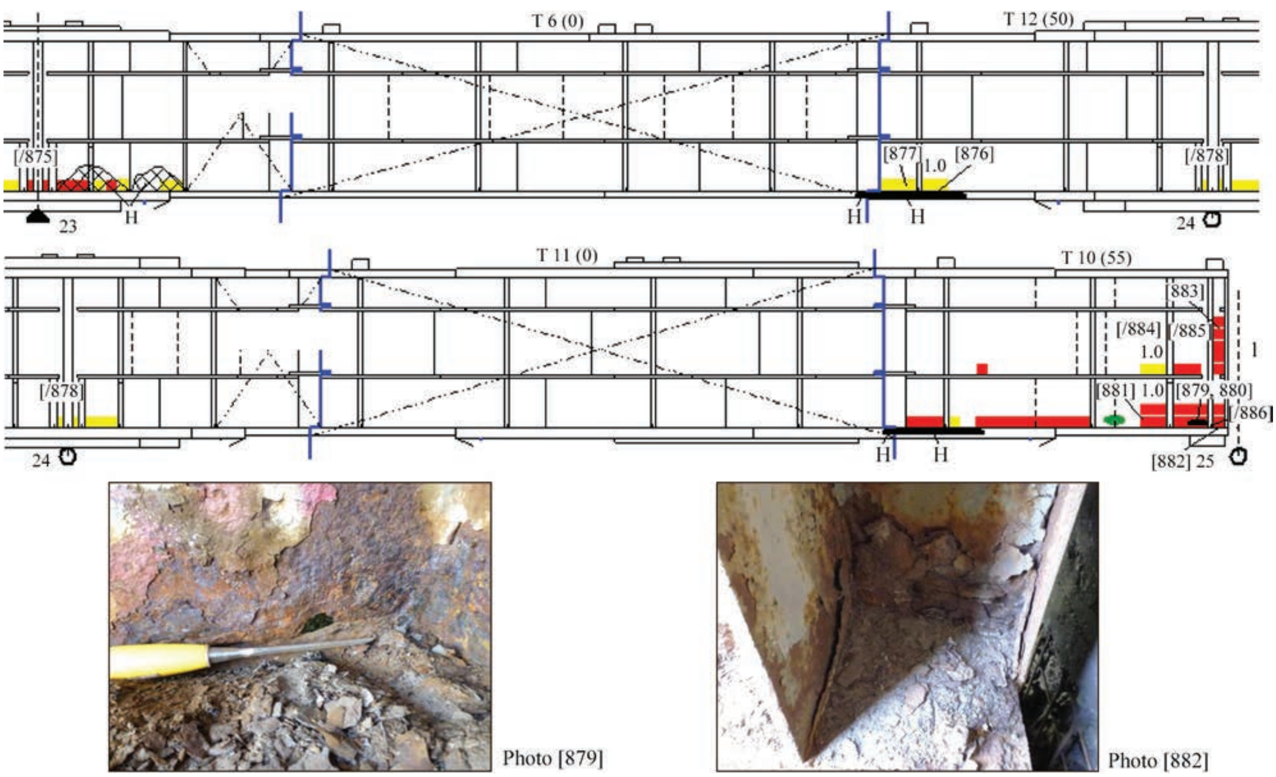

Figure 13. Fragment of tabulated results of testing elements of the beam No.1 of the four-span structure located between the 21–25 support

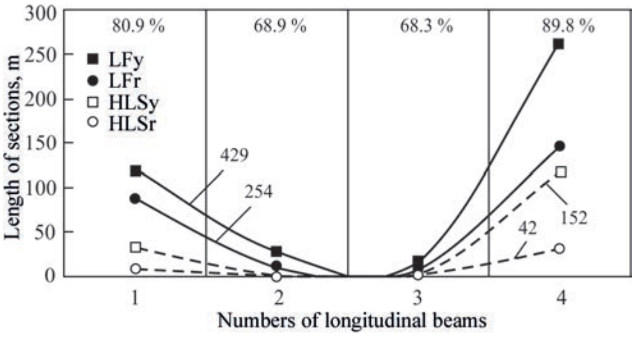

Figure 14. Total length of detected corrosion damages of the main longitudinal beams in the welding assemblies of the following elements: middle wall of the truss to the lower horizontal stiffener — HLS (y, r); lower wall to the lower flange of the truss — LF (y, r) (marks «y» and «r» characterize the depth of corrosion damages from 2.0 to 4.0 mm and more than 4.0 mm, respectively)

loss of metal from corrosion is in the range from 2 to 4 mm are yellow and red where it is more than 4 mm. A number above the color indicates the approximate length of the corresponding area along the truss. A separate square of yellow or red colour corresponds to a length of about 100 mm. If the area is separated by structural elements, such as for example vertical stiffeners or welded sheet joints, then a number above the color is not marked. Nonmetallic inclusions are green. The boundaries of trusses are marked in blue. Movable and immovable supports are respectively — ○ 22 △ 23. In square brackets, the numbers of photos of some sections are given. The sections that were not subjected to a selective testing are marked with dotted intersection. Defects are marked in black according to the data of LLC «V.N. Shimanovsky Ukrainian Institute of Steel Construction», given in the report compiled based on the results of the inspection of the bridge in 2018.

According to the results of selective measurements of the thickness of truss elements and the carried out analysis [9], it was determined that as a result of rainwater and moisture, formed by melting snow (containing salts), leaking through expansion welds of a reinforced concrete slab on the metal structures of the main beams, the metal in some regions of trusses suffered significant local corrosion damages. In some cases, the thickness of the metal as a result of corrosion in the lower girths, lower horizontal stiffeners and in the lower part of the walls of the main beams decreased significantly (in some cases by 40–50 %).

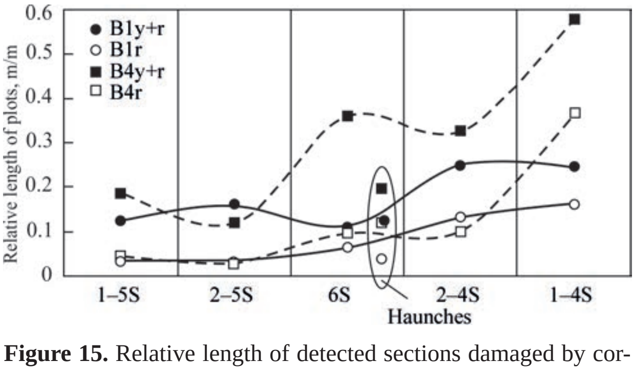

Figure 15. Relative length of detected sections damaged by corrosion in the welding-on assembly of the lower wall to the lower flange of the truss for the structures 1–5S; 2–5S; 6S; 2–4S; 1–4S of the end beams No.1 and No.4 to the controlled length of the structures (B1y+r is the total length of damages with a depth of more than 2.0 mm of the beam No.1; BБ1r is the total length of damages with a depth of more than 4.0 mm of the beam No.1; B4y+r is the total length of damages with a depth of more than 2.0 mm of the beam No.4; B4r is the total length of damages with a depth of more than 4.0 mm of the beam No.4)

The smallest depth of corrosion damages was observed near the expansion joints in the trusses of the middle main beams No.2 and No.3, where debris was absent (Figure 14). In addition to the sections of the main beams No.2 and No.3, located near the expansion joints, other elements of these beams are in satisfactory condition.

The greatest loss of metal thickness as a result of corrosion was found in the trusses of the end main beams No.1 and No.4 (Figures 14, 15). The main cause for such a damage was the presence of debris on the lower horizontal stiffener and the lower girth of these beams, which retains moisture (Figures 8–13).

The maximum corrosion damages to the elements were detected in trusses T10 and T15 of the four-span structure of the main beam No.1 and trusses T1 and T3 of the four-span structure of the main beam No.4. In these trusses deep corrosion damages (rust-through in some places, Figure 13), which need urgent repair.

It should be noted that during the works, the specialists of the PWI were provided with a limited access to the testing elements of longitudinal main beams in connection with a general unsatisfactory condition of the inspection passages and also with the debris accumulation on the end beams, which allowed performing only a partial inspection.

Thus, Figure 16, *a*, *b* shows a dependence of the detected corrosion-damaged areas of the inspected structures, where in the top of the diagram the percentage of the performed testing on the structures is indicated.

Taking into account the limited access to the structural elements, it is possible to evaluate to some extent the «expected» length of damaged sections of the structures on other beams. As an example, Figure 17 shows the predicted (expected) length of corrosion-damaged areas of strucutres in the places of welding the lower girth to the wall of the main beams No.1 and No.2.

In this case, when evaluating the expected length of corrosion damages to the beams B1 and B2, a linear extrapolation between the found damaged sections and the controlled length was used. This approach provides only an approximate evaluation of possible damages, but can be useful when planning future repair works. A more accurate evaluation of damages

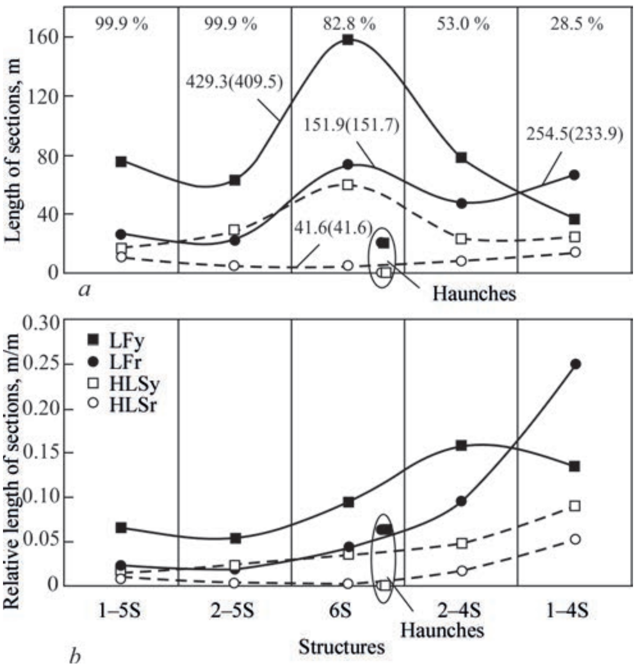

Figure 16. Length of detected sections damaged by corrosion of structures and percentage of performed testing (percentage of testing is indicated above) (*a*) and the relative length of detected sections damaged by corrosion of structures to the controlled length (*b*). The numbers indicate the total length, taking into account the data on haunches (in parentheses — without haunches)

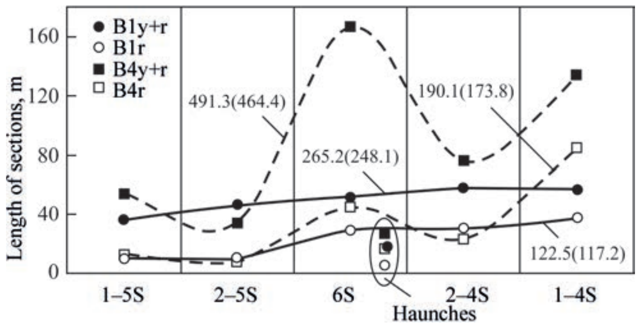

Figure 17. Example of predicting length of of detected sections damaged by corrosion in the welding-on assembly of the lower wall to the lower flange of the truss for the structures 1–5S; 2–5S; 6S; 2–4S; 1–4S of the end beams No.1 and No.4 (designation of curves as in Figure 15)

requires other approaches using probable methods. Thus, Figure 18 shows diagrams of distribution of detected damages to the trusses in the assemblies of welding-in the lower girt to the lower wall between the supports for the main beams No.1 and No.4. From the analysis of the results of this diagram it was found that the sections of detected damages are chaotic. The only similar pattern is an increase in damages along the boundaries of the structures.

Summarizing the results of the inspection of the main beams of the E.O. Paton Bridge across the Dnipro River in Kyiv, the following conclusions can be drawn.

1. Welded joints of truss elements of the main longitudinal beams are in satisfactory condition. In the course of a long operation, inadmissible defects and fatigue cracks were not formed in them.

2. As a result of leaking rainwater and water formed from melting snow (containing salts) on metal structures of the main beams, the metal of the end sections of the trusses adjacent to the expansion welds, suffered local but sometimes significant corrosion damages. As a result of corrosion, the thickness of the metal in the structural elements, namely of the lower girths, the lower horizontal stiffeners and in the lower

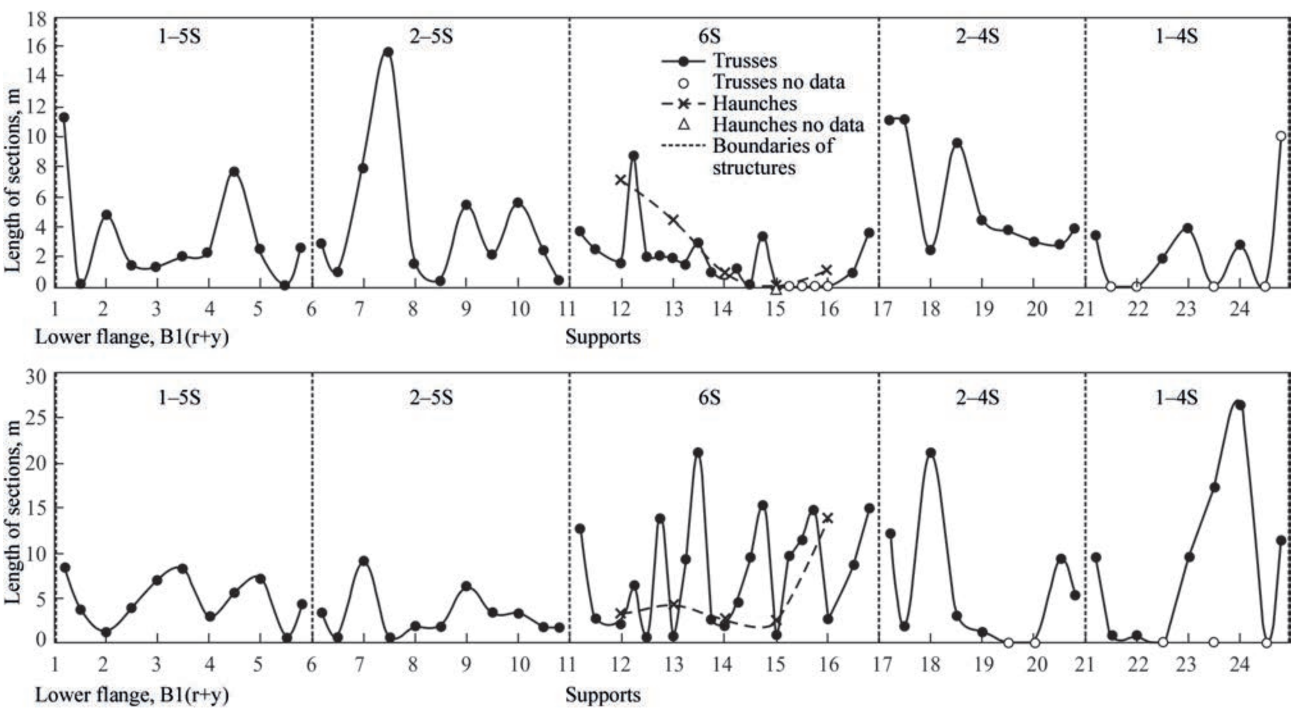

Figure 18. Distribution of detected damaged sections in the welding zone of the lower girth to the truss wall between the supports for the main beams No.1 and No.2 (designation as in Figures 15, 17)

part of the walls of the main beams significantly decreased. In some cases by 40–50 %.

3. The smallest corrosion damages are observed near the expansion welds in the trusses of the middle main beams No.2 and No.3, more intense are in the trusses of the end No.1 and No.4 main beams, which is caused by the debris accumulation on the lower horizontal stiffener and the lower girth of these beams, which retains moisture.

4. Local corrosion damages were formed on the lower flanges, lower horizontal stiffeners and parts of the truss walls of the end main beams No.1 and No.4 adjacent to them. The similar sections of the main beams No.2 and No.3 are in satisfactory condition.

5. The deepest corrosion damages (in some places through) were observed in the trusses T10 and T15 of the main beam No.1 and the trusses T1 and T3 of the main beam No.4. These trusses need urgent repairs.

6. Taking into account the current technical condition of the main beams of the E.O. Paton Bridge across the Dnipro River in Kyiv, on the condition that the works aimed at restoring their initial load-carrying capacity will be performed, the main beams can be used during reconstruction (restoration) of the bridge.

1. Anderson, W.E. (1969) *An engineer views brittle fracture history*. Boeing rept.
2. Biggs, W.D. (1960) *The brittle fracture of steel*. Mc. Donald and Evans.
3. (1953) *Report on prefabrication of span elements of Kiev city bridge at Dniepropetrovsk Molotov Plant.* Kiev, PWI library [in Russian].
4. (1953) Report on site welding of spans of Kiev E.O. Paton bridge across the Dnieper. *Ibid*. [in Russian].
5. Lobanov, L.M., Kyrian, V.I. (2013) The E.O. Paton allwelded bridge is sixty years old. *The Paton Welding J.*, **12**, 33–38.
6. Lobanov, L.M., Kirian, V.I., Shumitsky, O.I. (2003) Fifty years of the E.O. Paton bridge. *Ibid*., **10–11**,12–20.
7. Shimanovskyi, O.V., Kotlubei, D.O., Shalinskyi, V.V. (2018) The E.O.Paton bridge: Current state and prospects. *Promyslove Budivnytstvo ta Inzhenerni Sporudy*, **1**, 2–9 [in Ukrainian].
8. Shimanovskyi, O.V., Kotlubei, D.O., Shalinskyi, V.V. (2018) Emergency situation of the E.O.Paton bridge and measures for its solution. *Ibid*., **4**, 30–33.
9. Poznyakov, V.D., Dyadin, V.P., Davydov, Ye.O., Dmytrienko, R.I. (2021) Technical state of metal structures of the main spans of E.O. Paton bridge across the Dnipro in Kiev. *Ibid*., **1**, 9–17 [in Ukrainian].
10. (1989) *Textbook on design of reinforcement of steel structures (to SNiP II-23-81*).* Ukrniiproektstalkonstruktsiya. Moscow, Stojizdat [in Russian].

Received 03.06.2021

UNIT FOR HIGH-VELOCITY ELECTRIC ARC SPRAYING

> The unit is designed for deposition of wear, corrosion resistant and special coatings, repair of worn machine parts by means of double-wire electric arc spraying in high-velocity flow of hot combustion products of hydrocarbon gas with air of current-conducting materials in form of wire (flux-cored wire) of 1.6–2.2 mm diameter. Joint development of PWI and «PLAZER» Company.

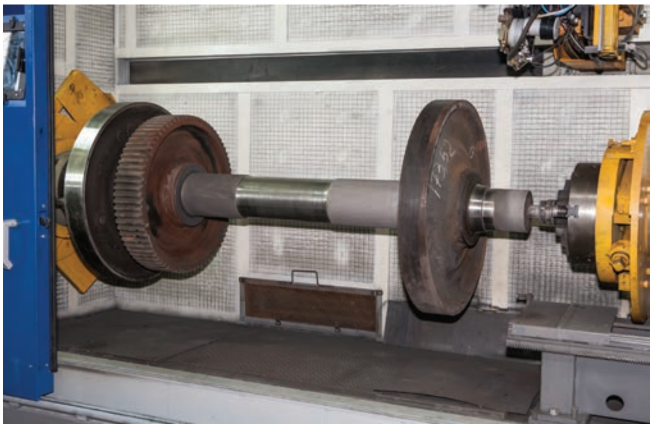

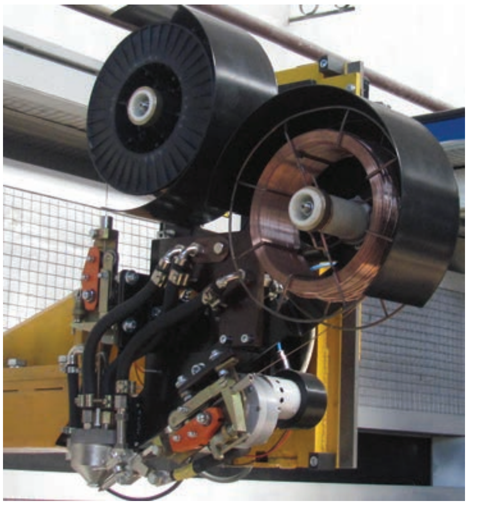

Block of high-velocity electric arc metallizer

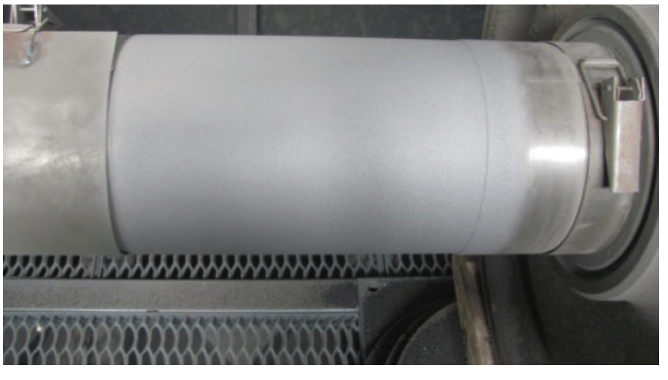

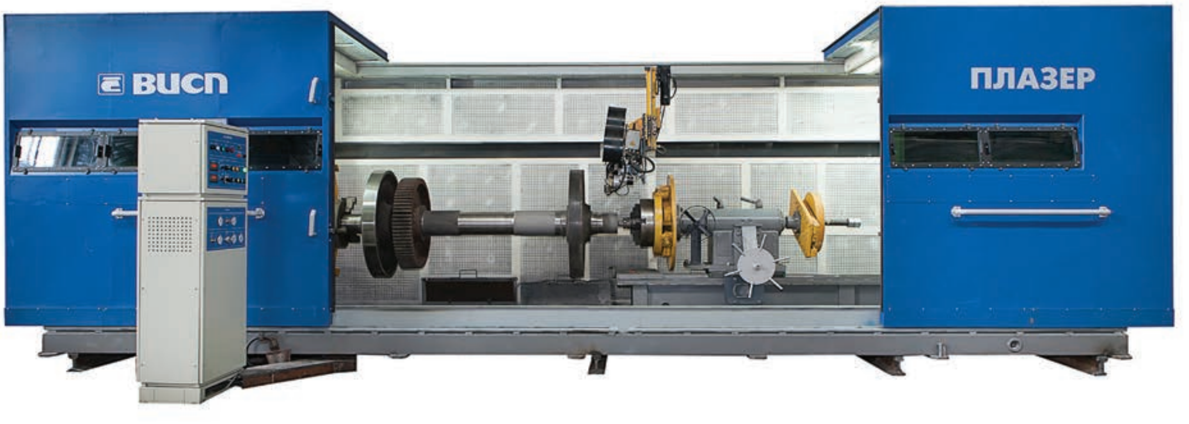

Appearance of restored part and unit in the framework of semi-automatic line

Developed by PWI

INDUCTION HIGH-FREQUENCY UNIT

FOR REMELTING OF REFRACTORY POWDER MATERIALS

One of the perspective directions of HF-plasma application is remelting of powder materials. A source of HF-discharge is a high-frequency generator, which induces a powerful electromagnetic high-frequency field in the inductor. The inductor contains a plasmatron forming a set mode for plasma forming gas escape at 7000–10000 °C temperature.

One of the directions of HF-plasma application is remelting of powder materials with further deposition of molten particles on a substrate; the second one is remelting and balling of powder materials. High melting efficiency of oxide materials allows wide application of developed equipment in additive technologies.

> Technology of plasma treatment of powder materials using HF-plasma allows receiving the spherical particles independent on shape of raw material. Application of special design reactor allows treatment of powder of chemically active metals and alloys in plasma with their further usage for additive technologies.

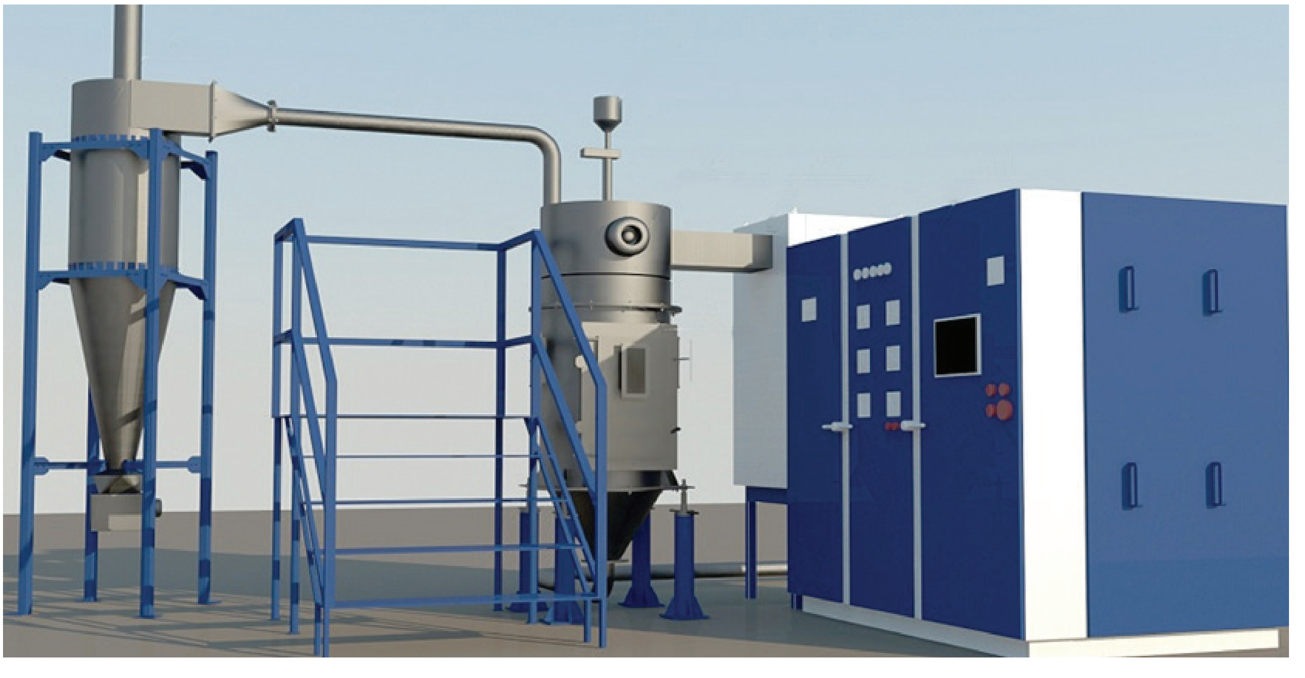

Developed by PWI

LASER TECHNOLOGY AND EQUIPMENT FOR MANUFACTURE OF MULTILAYER BELLOWS

PWI has developed the technology and equipment for laser welding of thin-wall pipes of stainless steel for manufacture of multilayer bellows, which carry and divide liquid and gaseous media, including aggressive ones.

Following the developed technology the bellow consists of several laser-welded thin-wall pipes (from 3 to 10 layers) of 0.15–0.20 mm thickness each. The bellow will keep working capacity in such a multi-layer bellow structure, even if one welded joint breaks in process of operation.

Development advantages:

- reduced amount of rejects from 50 % in argon-arc welding to 0.5 % in laser welding
- 4 times rise of productivity
- cyclic strength, corrosion resistance and other characteristics of laser-welded multilayer bellow 1.5–4 times exceed the characteristics of single layer bellow made by argon-arc welding (depending on number of layers and bellow sizes).

Developed by PWI

WELDING OF TITANIUM

AND ITS ALLOYS

A team of experts in the field of welding of titanium and alloys on its basis has been working at PWI for more that 30 years. For the first time in the world the unique technologies of non-consumable argon-arc welding of titanium with halogenide fluxes; narrow-gap argon-arc tungsten electrode welding with controlling magnetic field; press welding of titanium with copper and aluminum with steel were developed in course of these years.

The technologies for titanium and its alloys welding developed at the PWI have found wide application in aircraft- and rocket construction as well as at enterprises of chemical machine building of CIS countries. Currently, PWI fulfills contract-based complex works on development of technology and equipment for titanium welding and engineering maintenance at manufacture of specific products.

Developed by PWI

MICROPLASMA SPRAYING
OF BIOCOMPATIBLE COATINGS ON IMPLANTS

PWI has developed a technology and equipment of microplasma spraying of biocompatible coatings on the surface of different implants, including hip implants, dental implants, intervertebral cages etc.

Unit for microplasma spraying MPN-004 with powder batchbox

This technology allows depositing coatings from hydroxyapatite powder (HA), titanium cellular coatings as well as double-layer biocermet (titanium-hydroxyapatite) coatings. Spraying of biocompatible coatings is done on microplasma spraying unit MPN-004. PLASMATRON FOR SPRAYING OF COATINGS Pub. No.:WO/2004/010747, International Application No.: PCT/UA2003/000014, Publication date: 29.01.2004. (IRP4).

Spraying of Ti-layer with regulated porosity (5–30 %, pore size 50–300 μm) and minimum oxidation level is carried out by means of microplasma spraying of Ti-wire. Combination of cellular Ti-coating with external HA layer provides coating cohesion strength with implant surface satisfying ISO 137779-2 and high level of biocompatibility.

> Based on complete complex of mechanical and biomedical tests the implants with microplasma biomedical coatings are used in practice for hip replacement.

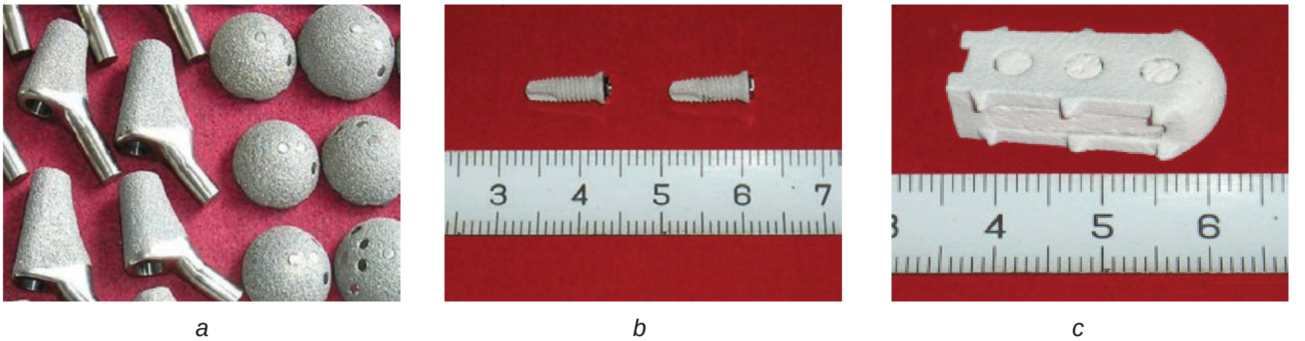

a *b* *c*

Products with biocompatible coatings made by microplasma spraying: *a* — parts of hip implant; *b* — cermet implant for interbody spinal fusion; *c* — dental implant

Developed by PWI

Calendar of July *

JULY 1, 2000 Entered into force Rules for classification and construction (Materials and Welding). These Rules apply to all welding work performed in the course of new construction, conversion or repairs carried out on ships and their machinery installations, including steam boilers, pressure vessels and pipelines, for which an application for classification has been submitted to Germanischer Lloyd.

JULY 2, 1929 American inventor and businessman Edward Budd (1870–1946) received a patent on the technology of welding in the automotive industry. Edward Budd was a pioneer in the mass production of all-metal car bodies and founded his own company «Edward Budd Manufacturing Company». Preferring the frame metal structures, Edward Budd proceeded not only from the fact that they are stronger than wood ones and also more manufacturable. Edward Budd was the first who applied spot welding in the automotive industry.

JULY 3, 1960 At the beginning of July 1960, T.M. Slutskaya (1907–1987), a representative of the Paton School, developed for the first time the self-shielding activated electrode materials for arc welding. She developed the basis of alloying wires with rare earth and rare metals, due to which nitrogen was bound into refractory nitrides.

JULY 4, 1981 The largest Soviet nuclear-powered submarine in the world, a heavy strategic-purpose missile cruiser submarine of the Project 941 «Akula» with a length of more than 170 m was put into tests. Its pressure hulls were welded from sections (shells) of cylindrical, conical and elliptical shape with a wall thickness of 75 mm. A similar submarine at the same time was created in the United States and, later on was named «Ohio».

JULY 5, 1931 Date of death of Oscar Chelberg (1870–1931), a Swedish inventor and industrialist, founder of the company ESAB in 1904. Oscar Chelberg invented the electrode coating used for manual arc welding by immersion of a bare steel wire into the mixture of carbonates and silicates. The purpose of the coating is to protect the molten metal from the effect of oxygen and nitrogen, present in the atmosphere. His pioneering developments laid the foundation for beginning the investigations on the development of reliable welding electrodes. Today, ESAB produces welding materials, equipment for welding and cutting of metal for practically all the branches of industry.

JULY 6, 1935 The construction of the German heavy cruiser «Admiral Hipper» was started. After signing the Treaty of Versailles, Germany was restricted in the construction of large-capacity ships. In order to officially comply with the restrictions to weight, several radical innovations were included in the design of this type of a ship. Designers were the first to use welding in large military ships instead of riveting. Because of their heavy armament of eight 203 mm guns and small sizes, the British began referring to such vessels as «pocket battleships». The hull of the ship was built of transverse steel frames; more than 90 % of the structure was joined using welding, which reduced the total mass of the hull by 15 %.

JULY 7, 1962 The absolute speed record of 2681 km/h was set in the experimental all-weather interceptor E-166 of the Design Bureau «MiG». This flight was performed by the test pilot G.K. Mosolov. Unlike the Americans, who chose a titanium alloy as the basic material of their reconnaissance aircraft, the «Experimental Design Bureau named after A.I. Mikoyan» chose different grades of steels. Its application allowed refusing from riveted structures in favour of welded ones. This, in turn, required the creation of new technological cycles, taking into account the use of different welding methods during a large-panel assembly. The experimental operation of the E-166 aircraft allowed gaining an important flight experience at high supersonic speeds.

JULY 8, 1761 Date of birth of V.V. Petrov (1761–1834), a Russian physicist- experimenter, self-taught electrical engineer, academician of the St. Petersburg Academy of Sciences. One of the outstanding achievements of the scientist was the discovery of the phenomenon of an electric arc in 1802 and evidence of the possibility of its practical application for the purpose of melting, welding metals and their reduction from ores and for lighting. In 1802, he designed a large galvanic battery consisting of 2100 copper-zinc cells with an electromotive force of about 1700 V.

*The material was prepared by the Steel Work Company (Krivoy Rog, Ukraine) with the participation of the editorial board of the Journal.

JULY 9, 2014 The first launch of the rocket-carrier of «Angara» family from the «Plesetsk» Cosmodrome was performed. The rocket is capable of delivering 35 tons of cargo into orbit. The requirements of strength and tightness of welds of the fuel tanks were the most fully satisfied by argon-arc welding. During the construction of the «Angara» rocket -carrier, it is supposed to gradually introduce friction stir welding for application. The «Angara» rocket-carrier replaces the outdated model «Proton-M».

JULY 10, 1905 During dispersal of the workers meeting, L.I. Borchaninov (1837–1905) was killed. He was a worker at the Motovilikh plants, one of the first welders in Russia. He was working under the supervision of N.G. Slavyanov, an inventor of arc welding of metals. Together with the worker P. Aspidov, he accompanied Slavyanov to the Fourth Electrical Exhibition in St. Petersburg, where they equipped a temporary workshop and demonstrated the process of restoring metallic parts using electric welding. He participated in the building of the largest in Russia and Europe tugboat «Kasogs Prince Rededya», where welding was used instead of riveting for the first time in the history of shipbuilding.

JULY 11, 1979 «Skylab», the first and only American space station, leaved the orbit, completing its work. During the flight, experiments were carried out on evaluation of the effect of zero gravity on the quality of welded joints produced by electron beam welding. The «Skylab» station was equipped with a complex which included multi-purpose electric furnaces and an electron beam installation. The experiments were conducted on the investigation of molten metal, photographing the behaviour of calcined materials in zero gravity, studying the crystal growth, treatment of immiscible alloys and brazing of stainless steel.

JULY 12, 1929 The first in the history of aviation the flight of the German giant flying boat «Dornier Do-X» took place. The aircraft was designed for service at the long-distance passenger airlines. On October 20, 1929, during a 40-minute demonstration flight, this plane took off from the Lake Constance with 169 passengers on board. This record remained unsurpassed in the first half of the XX century. Due to the low flight characteristics, the aircraft did not come to the series production but only made several demonstration flights to Africa, North and South America in 1930–1932. In order to reduce weight, welding was applied for joining aluminum parts.

JULY 13, 1936 The destroyer of the project 7 «Gnevny» was launched. It was the main ship of the so-called Stalinist series, built for the Soviet Navy in the second half of the 1930s, one of the most popular types of destroyers in the history of the Soviet fleet. The thickness of the hull lining was 5–9 mm, the deck flooring was 3–10 mm, and the watertight bulkheads were only 3–4 mm. The structures were mainly riveted, but the electric welding was used for the assembly of bulkheads, platforms under the lower deck and a number of other elements.

JULY 14, 1969 An inhabited underwater apparatus designed to study the middle depths of the Gulf Stream (up to 1000 m), the Ben Franklin mesoscaphe, was submerged into the water. It was designed by Jacques Picard. A special attention was paid to welds. Numerous tests and examinations were carried out before it was allowed to use the apparatus. For welding, electrodes, alloyed with manganese and molybdenum, were used.

JULY 15, 2010 In the summer of 2010, the book «Paton School» was prepared for publication. It presents information about the world-famous Paton's scientific and engineering school in the field of welding and related technologies, which was organized by academician E.O. Paton, an outstanding scientist, and further developed by academician B.E. Paton, a worthy successor of his activities. In the book the formation and development of this school is highlighted and information about its famous representatives is given.

JULY 16, 1961 By decree of the Presidium of the Supreme Soviet of the USSR for great successes in the development of the rocket industry, science and technology, successful performance of the first flight of a Soviet man in space in the «Vostok» spacecraft-satellite, M.K. Yangel was re-awarded the title Hero of Socialist Labour.

JULY 17, 1964 By resolution of the Council of Ministers of the Ukr.SSR of 12.06.1964 No. 59.5 and resolution of the Presidium of the Academy of Sciences of the Ukr.SSR of July 17, 1964 No. 188 the E.O. Paton Prize of the National Academy of Sciences of Ukraine was established for outstanding scientific works in the field of developing the new metallic materials and methods for their treatment. This is one of the few examples where the award is named after a welder-scientist.

JULY 18, 1955 At Disneyland an amusement facility: a model of a space rocket called Moonliner, was opened. Since 1955 to 1962 Moonliner was located in the first futuristic exhibition. It was also an example of a new approach to modern advertising media. In order to build a 27-meter aluminum rocket the welding in inert gases was used. It is interesting that with the development of rocket construction, the same welding methods were used in the production of real space rockets. The construction of such a facility caused a wide resonance with the public already before the launch of the first satellite of Earth.

JULY 19, 1900 The opening of the Paris Metro took place. The opening was dated for the beginning of the 1900 World's Fair. The Paris Metro is one of the oldest metros in Europe (the fourth after the London, Budapest and Metro in Glasgow). The unsurpassed capabilities of thermit welding at that time were demonstrated visually during laying the tracks of the Paris Metro.

JULY 20, 1966 The crew commander Neil Armstrong and the pilot Edwin Aldrin of the American spacecraft «Apollo-11» landed a lunar module on the Moon. The accomplishment of this project could not be achieved without the use of modern welding technologies.

JULY 21, 2007 The skyscraper «Burj Khalifa» of 829.8 m height was officially recognized as the tallest building in the world during construction. The solemn opening ceremony took place on January 4, 2010 in Dubai, the largest city of the United Arab Emirates. During its construction the welding technologies were especially in demand. They were applied starting from the foundation and ending at the highest point, where everything was fastened either with bolts or electric arc welding. It is one of the records and demonstrates how large structures can be created by welding. The spire of «Burj Khalifa» is a complex steel structure with many columns and welded beams.

JULY 22, 1872 Date of birth of V.F. Mitkevich (1872–1951), an outstanding Russian and Soviet electrical engineer, academician of the Academy of Sciences of the USSR. In 1901, he proposed circuits of a single-phase full-wave rectifier (full-wave with two windings) for converting an alternating current into a direct current and a three-phase one-half-wave rectifier (half-wave with zero output). V.F. Mitkevich was the first in the world to propose a three-phase arc for welding metals.

JULY 23, 1995 Date of death of N.A. Langer (1910–1995), a chemical scientist-analyst, representative of the Paton school. He made a significant contribution to the development of methods for protection of welded joints against corrosion. He proposed original electrochemical methods for studying the corrosion resistance of welded joints. They allow predicting the stability of joints during operation in the environments with a high corrosion activity. Langer investigated the conditions for the occurrence of particularly threatening corrosion of welded joints, the so-called crevice corrosion, and also identified methods for its elimination. The results of a number of works have found application in industry.

JULY 24, 1967 In St. Louis the Arch was opened, also known as a Gateway to the West. It is a memorial, which is the hallmark of St. Louis. Its height is 192 m at the highest point and the width of its base is also 192 m. The arch is the highest monument at the territory of the United States. Builders, together with the company «Lincoln Electric», successfully manufactured and joined 142 parts of one of the most complex building structures in the US history. During its construction the manual arc welding, semi-automatic gas-shielded welding and submerged-arc welding were used.

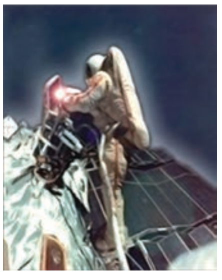

JULY 25, 1984 In open space outside the board of the orbital station «Salyut-7», experiments in electron beam welding were carried out using a welding device URI (a versatile hand tool) designed at the E.O. Paton Electric Welding Institute. This device allowed welding, cutting, brazing metal and depositing coatings. The cosmonauts V. Dzhanibekov and S. Savitskaya went into outer space to perform welding technological works. For three and a half hours, the cosmonauts conducted the entire complex of planned experiments.

JULY 26, 1845 The ship «United Kingdom» with an all-metal hull started its first voyage across the Atlantic. The vessel was distinguished by its enormous sizes: its length was almost 100 m. In the «United Kingdom» for the first time, a screw propeller was used instead of paddle-wheels. That was a real event in shipbuilding. When creating a huge crankshaft for the ship, a new modernized «welding hammer» was used, invented by Joseph Stenster.

JULY 27, 1942 The American interceptor «Mustang NA-73X» took the first air battle. The need in accelerated production of military machinery forced the use of welding even wider. It was estimated that during the transition to welding in an aircraft weighing 4 tons, where it was usually necessary to apply up to 100,000 rivets of 112.5 mg each, a weight reduction of about 10 % is achieved. At the same time, aerodynamics, tightness and corrosion resistance are improved, and the time for manufacturing the whole structure is shortened by 60 %.

JULY 28, 1883 Date of birth of V.P. Vologdin (1883–1950), a Soviet scientist and engineer, a pioneer in the use of electric welding in ship building. He designed and built the first all-welded ship in the USSR. A tugboat of the series «ZhS» (iron welded) was built. It turned out that a hull of the ship became lighter, the labour intensiveness of the ship building was reduced by a third.

JULY 29, 1993 A certificate on registration of the Society of Welders of Ukraine was issued. It was founded in November 1992 by the initiative of the E.O. Paton Electric Welding Institute (Kiev). The organization unites all scientists, teachers, specialists, craftsmen and workers in the field of welding and related processes in Ukraine. The main task of the Society is informational, consulting, legal support of all workers employed in the welding industry of Ukraine.

JULY 30, 1904 The longest battle of the Russian-Japanese War, the defence of Port Arthur (July 30–December 23, 1904) began. The sailors of the Russian fleet and the workers of the Baltic Ship Repair Plant, located in the besieged city, successfully used arc welding by a coal electrode to repair the ship hulls.

JULY 31, 1962 Date of death of Nils Miller (1899–1962). He left after him a large company «Miller Electric». In the 1920s almost all electric arc welding was carried out using a bulky and expensive three-phase generator. In 1929, Nils Miller realized the need in designing a small and inexpensive welding machine, operating from the power mains. In 1935, the company «Miller Electric» was founded. Next year, El Mulder, the chief engineer of the «Miller Electric», invented the first in the world high-frequency industrial welding device at alternating current. This invention significantly improved the quality of welding and allowed using welding at alternating current.

SUBSCRIPTION–2021

«The Paton Welding Journal» is Published Monthly Since 2000 in English, ISSN 0957-798X, doi.org/10.37434/tpwj.

«The Paton Welding Journal» is Cover-to-Cover Translation to English of «Automatic Welding» Journal Published Since 1948 in Russian and Ukrainian.

«The Paton Welding Journal» can be also subscribed worldwide from catalogues subscription agency EBSCO.

If You are interested in making subscription directly via Editorial Board, fill, please, the coupon and send application by Fax or E-mail.

12 issues per year, back issues available.

$384, subscriptions for the printed (hard copy) version, air postage and packaging included.

$312, subscriptions for the electronic version (sending issues of Journal in pdf format or providing access to IP addresses).

Institutions with current subscriptions on printed version can purchase online access to the electronic versions of any back issues that they have not subscribed to. Issues of the Journal (more than two years old) are available at a substantially reduced price.

SUBSCRIPTION COUPON

Address for journal delivery ____________________

Term of subscription since ________ 20 ____ till ________ 20 ____

Name, initials ____________________

Affiliation ____________________

Position ____________________

Tel., Fax, E-mail ____________________

The archives for 2009–2019 are free of charge on www://patonpublishinghouse.com/eng/journals/tpwj

Address
11 Kazymyr Malevych Str. (former Bozhenko Str.), 03150, Kyiv, Ukraine
Tel.: (38044) 200 60 16, 200 82 77
Fax: (38044) 200 82 77
E-mail: journal@paton.kiev.ua